Preliminary Report on Engineering and Geological Effects of the July 2019 Ridgecrest Earthquake Sequence

A report of the NSF-Sponsored Geotechnical Extreme Event Reconnaissance Association

GEER Team Members

Scott J. Brandenberg, Pengfei Wang, Chukwuebuka C. Nweke, Kenneth Hudson, Silvia Mazzoni, and Yousef Bozorgnia, UCLA

Christine A. Goulet, Southern California Earthquake Center

Kenneth W. Hudnut, USGS

Craig A. Davis, Retired, City of Los Angeles Department of Water and Power

Sean K. Ahdi, Exponent, Inc. and UCLA

Farzin Zareian and Jawad Fayaz, UC Irvine

Richard D. Koehler, Colin Chupik, and Ian Pierce, University of Nevada, Reno

Alana Williams, Arizona State University

Sinan Akciz, CSU Fullerton

Martin B. Hudson, Wood.

Tadahiro Kishida, Khalifa Univ. of Science and Technology, UAE, Visiting Scholar, UCLA

Collaborating Authors

Ben Brooks, Ryan Gold, Dan Ponti, Katherine Scharer, Devin McPhillips, Chris DuRoss, and Todd Ericksen, USGS

Janis Hernandez, Jay Patton, Brian Olson, Tim Dawson, Jerome Treiman, California Geological Survey

Kelly Blake, Geothermal Program Office, US Navy

Jeffrey Bachhuber, Chris Madugo, and Joseph Sun, Pacific Gas & Electric Company, Geosciences Division

Andrea Donnellan, Greg Lyzenga, Erik Conway, Jet Propulsion Laboratory (JPL), California Institute of Technology

GEER Team Leader and Report Editor: Jonathan P. Stewart, UCLA

Report GEER-064: https://doi.org/10.18118/G6H66K

July 19 2019. Revised 8/1/2019

Acknowledgments

The work of the GEER Association, in general, is based upon work supported in part by the National Science Foundation through the Geotechnical Engineering Program under Grant No. CMMI-1826118. Any opinions, findings, and conclusions or recommendations expressed in this material are those of the authors and do not necessarily reflect the views of the NSF. Any use of trade, firm, or product names is for descriptive purposes only and does not imply endorsement by the U.S. Government. The GEER Association is made possible by the vision and support of the NSF Geotechnical Engineering Program Directors: Dr. Richard Fragaszy and the late Dr. Cliff Astill. GEER members also donate their time, talent, and resources to collect time-sensitive field observations of the effects of extreme events. Sponsorship of this GEER deployment was also provided by the Natural Hazards Risk and Resilience Research center (NHR3) and the Southern California Earthquake Center. Portions of this work were carried out at the Jet Propulsion Laboratory, California Institute of Technology under contract with NASA.

Individuals that assisted the GEER team in data collection, report production, review, and related matters include:

- Naval Air Weapons Station, China Lake: Captain Paul M. Dale, Commanding Officer; Matt Boggs, Chief Engineer, China Lake Ranges, Naval Air Warfare Center, Weapons Division; Stephan Bork, Environmental Management Division; Margo Allen & Helen Haase, Public Affairs Officers; and Lt. 'Bill' Willard, Remote Range Supervisor
- Jed McLaughlin, Chief of Police, City of Ridgecrest
- Elizabeth Cochran, Alex Grant, Eric Thompson, Alan Yong, Jamie Steidl, David M. Boore (retired), Katherine Kendrick, and Shane Detweiler, USGS
- UAV team (UCLA): Timu Gallien, Maria Winters, Marie-Pierre Delisle, Joseph Lucey, and Yeulwoo Kim
- UAV team (UW Rapid site): Andrew Lyda, Sean Yeung. Assistance from Omar Issa, Tristan Buckreis, Zhengxiang Yi (UCLA)
- Shawn Barker, Shawn Barker Construction, Argus, CA
- Priscilla Benadom, Trona resident
- Dale Fuller, Ridgecrest resident
- Raymond Becker, Searles Valley Domestic Water
- Ken Santini, Santini & Associates, Tucson, Arizona
- Albert Kottke, Katie Herr, PG&E; Chris Hitchcock and Ozgur Kozaci, Infraterra
- Jeff Keaton and Wyatt Iwanaga, Wood.
- Albert Kottke and Chris Madugo, PG&E
- Xiafeng Meng, USC
- David Frost and Fangzhou (Albert) Liu, Georgia Tech

We extend special thanks to Niket Agrawal, Pinkal Panchal, Gabriel Martinez, Managers of Super 8 Motel, Ridgecrest, who gave GEER team members access to their breakfast room for meetings and provided security camera footage of shaking during the **M**7.1 earthquake.

TABLE OF CONTENTS

Acknowledgments **2**

1.0 Introduction **6**

2.0 Reconnaissance Activities and Preliminary Findings **7**

2.1 Surface Fault Rupture 9

Surface Fault Rupture Mapping North of Highway 178 10

July 4 2019 M6.4 Event 10

July 5 2019 M7.1 Event 12

Mapping South of Naval Base - Overview 23

M7.1 fault trace; detailed mapping 30

M6.4 fault trace; detailed mapping 34

Additional Ground Deformations 35

2.2 Lifeline Performance 37

Highways and Roads 37

Railroads 38

Water Systems 38

Wastewater Systems 42

Communications 42

Natural Gas 42

Liquid Fuels 44

Electric Power 44

Los Angeles Department of Water and Power 45

Dams and Reservoirs 45

Fire Following Earthquake 45

2.3 Liquefaction and Related Ground Failure 45

2.4 Ground Motions 53

Recorded Ground Motions 53

Temporary Arrays 58

Fragile Geologic Features 59

2.5 Structural Performance 59
NAWSCL Structures 61
Wood-frame Structures 61
Mobile homes 62
Hospital 64
Damage masonry components 66
Ridgecrest Cinema 67
Bridges 68
3.0 Imaging **69**
3.1 Digital Elevation Models (DEMs) from Photographs 69
3.2 Lidar 73
4.0 DesignSafe Integration **74**
References **75**

1.0 Introduction

The 2019 Ridgecrest earthquake sequence began in earnest on July 4 2019 at 10:33 am local time, when an **M**6.4 (per USGS) earthquake occurred near Indian Wells Valley, south of China Lake and west of Searles Valley, California (Figure 1). This **M**6.4 event occurred on a left-lateral NE-trending fault (roughly parallel with the Garlock fault to the south, within the Little Lake fault zone at a hypocentral depth of 11.7 km. The NE-trending structure is termed a cross-fault because it extends between longer NW-trending features, which are more prevalent in the region. Like the Garlock, the cross-fault slip was left-lateral, causing crustal movement to be away from, and therefore decompressing, the eventual mainshock epicentral portion of the NW-trending fault structure that intersects the cross-fault, as shown in Figure 1. Similarities are noted between "cross-fault triggering" aspects of this earthquake sequence and the Elmore Ranch - Superstition Hills earthquake sequence of 1987 (e.g., Hanks and Allen, 1989; Hudnut et al., 1989), for which that mechanism was originally hypothesized.

Aftershocks on July 4 2019 and for most of July 5 2019 occurred along the cross fault, but also began to migrate to the NW along the NW-trending strand. These increased into the afternoon and evening of July 5, including an **M**5.4 event occurring at 4:07 pm local time (USGS) on the NW-trending fault and an **M**5.0 event occurring at 8:16 pm local time (USGS). An **M**7.1 (USGS) event occurred shortly thereafter at 8:19 pm local time on the NW-trending fault at a depth of 8.0 km. The event hypocenter is north and west upstrike from most of the prior activity. The rupture occurred bilaterally to the NW and SE over an approximate length of 50 km (Figure 1). The **M**7.1 rupture was right-lateral strike-slip, similar to the plate boundary San Andreas fault located approximately 140 km to the southwest.

As shown in Figure 1, the Little Lake fault zone occurs in the Eastern California Shear Zone (ECSZ), within a region north of the Garlock fault and east of the Southern Sierra Nevada fault zone. This zone is undergoing crustal extension on normal faults near the westernmost extent of the Basin and Range tectonic province. Moreover, it is also experiencing right-lateral strike-slip shear deformation in the NW direction. The **M**6.4 earthquake may have reduced normal stresses on the NW-trending fault strand that later produced the **M**7.1 earthquake, perhaps after fluid diffusion and the resultant re-equilibration of pore stress, and an accompanying gradual decrease in the frictional strength in the eventual main fault nucleation zone (Hudnut et al., 1989). Since it was also close in space and time, the **M**6.4 event is considered a foreshock to the **M**7.1 event.

The earthquake significantly impacted the Naval Air Weapons Station China Lake (NAWSCL), where a large fraction of the surface rupture and the largest ground motions occurred. Also affected were the City of Ridgecrest to the west and the Searles Valley region to the east (including the town of Trona and a large mineral extraction operation in the mostly dry Searles

Lake). A number of lifelines cross the fault south of the base, spanning between Ridgecrest and Trona.

The NSF-funded Geotechnical Extreme Events Reconnaissance (GEER) association, with co-funding from the B. John Garrick Institute for the Risk Sciences at UCLA and support from the Southern California Earthquake Center (SCEC), mobilized a team to the region on July 5 to document perishable data on the **M**6.4 event effects. The GEER team experienced the **M**7.1 event after retiring to a motel in Ridgecrest. Work then continued over a one-week period in several phases, during which investigators undertook initial reconnaissance to identify major effects, performed detailed mapping of ground failure features, and conducted unmanned aerial vehicle (UAV) imaging.

The GEER team is multi-disciplinary, with expertise in geology, seismology, geomatics, geotechnical engineering, and structural engineering. Our approach was to combine traditional reconnaissance activities of on-ground recording and mapping of field conditions, with advanced UAV-based imaging of critical features. GEER collaborated extensively with other reconnaissance teams operating in the region, including a fault mapping team comprised of the U.S. Geological Survey (USGS), California Geological Survey (CGS), and U.S. Navy personnel and a UAV team from NASA. This report has been prepared jointly by GEER team members and members of those collaborating organizations.

The objective of this preliminary report is to provide an overview of the major earthquake effects in a timely way, as well as a description of activities undertaken by GEER and collaborating organizations (mainly USGS and CGS). Further findings reflecting additional data collection and analysis will be presented in subsequent publications.

2.0 Reconnaissance Activities and Preliminary Findings

Figure 1 shows the most strongly affected region. Our activities focused on the following aspects of the earthquake events:

1. Surface fault rupture
2. Lifeline performance
3. Liquefaction and related ground failure
4. Ground motions
5. Structural performance in Ridgecrest

Relatively little work was done on landslides. Some discussion of landslide interactions with lifelines (mainly roads) is provided in Section 2.2.

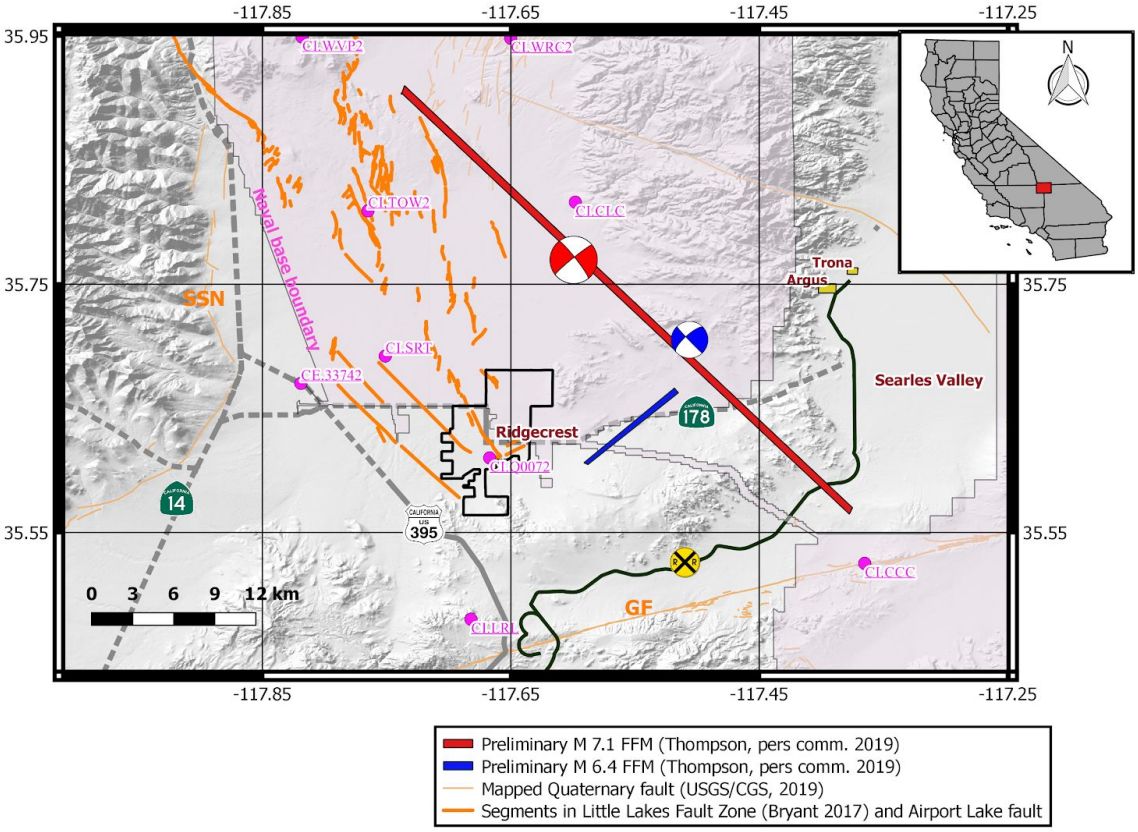

Figure 1. Regional map showing the Ridgecrest - China Lake - Searles Valley region along with mainshock event moment tensors, Little Lake fault zone traces, and other regional faults. Fault traces are based on USGS Quaternary Fault Database (USGS and CGS, 2019), Little Lake fault zone based on Bryant (2017). SSN = southern Sierra Nevada Fault, GF = Garlock fault. Surface projections of linearized preliminary finite fault models (FFMs) provided by E. Thompson (pers. communication, 2019). Developed areas affected by earthquakes are indicated (Ridgecrest, China Lake Naval Air Weapons Station, Trona).

2.1 Surface Fault Rupture

Both the **M**6.4 and **M**7.1 events produced substantial surface rupture. As shown in Figure 2, the **M**6.4 event ruptured the NE-trending left-lateral cross fault over a distance of approximately 9.5 km but evidently not the main NW-trending right-lateral fault, at least not at the surface. Seismicity did occur on a portion of the NW-SE oriented fault as well, forming an "L-pattern" in the seismicity that followed the M 6.4. The **M**7.1 event then ruptured the NW-trending main fault over a length of 50 km. Most of the **M**6.4 rupture occurred south of the NAWSCL (6.4 of 9.5 km) whereas most of the **M**7.1 rupture (36.5 of 50 km) occurred within the Naval Air Weapons Station, China Lake (NAWSCL).

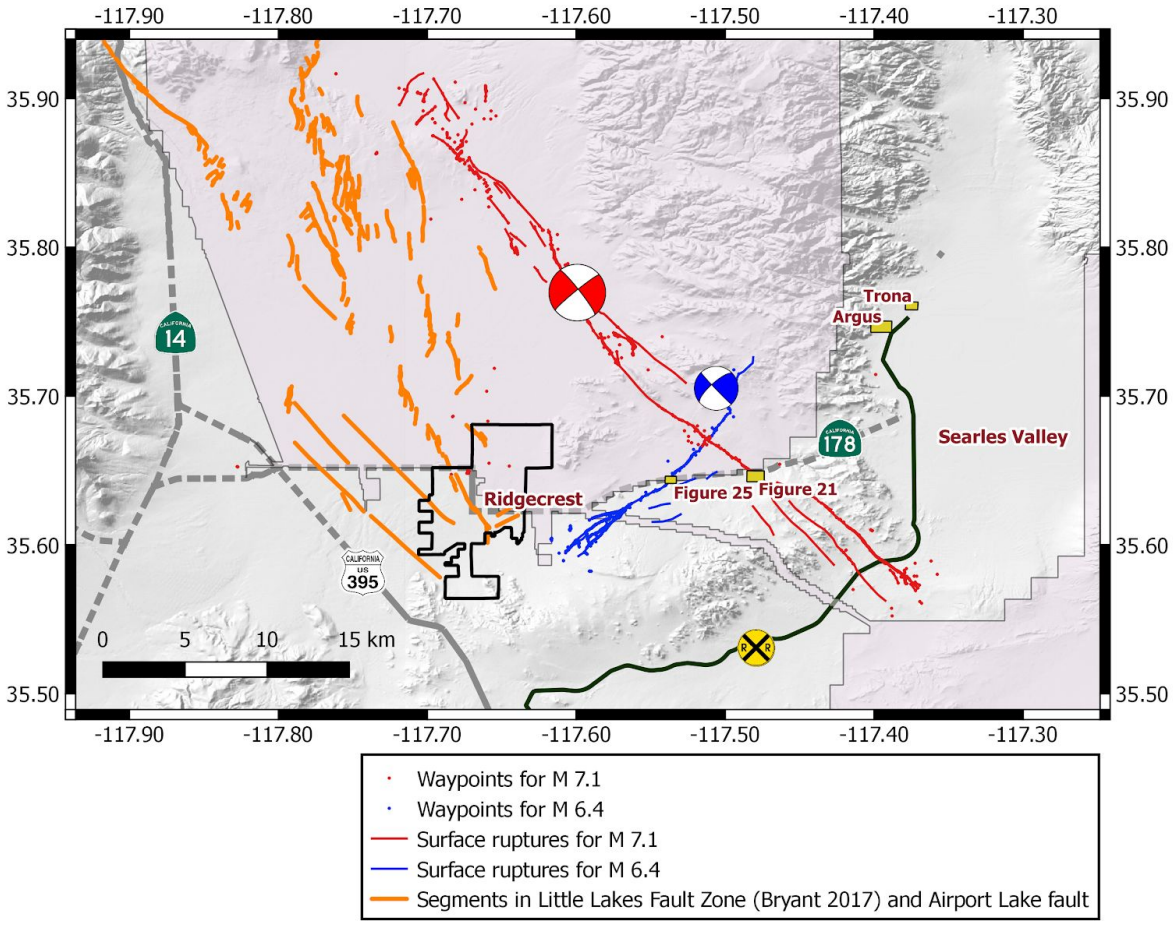

Figure 2. Provisional mapped surface ruptures and fault rupture observation waypoints of the **M**6.4 and **M**7.1 faults (shapefiles obtained from D. Ponti, 7/17/2019). Some of the waypoints may not be observations of fault rupture. The linear red and blue segments plotted on the map were constructed primarily based on ground observation locations, supplemented by interpretation of satellite interferometry correlation images from NASA's ARIA project to provide guidance for drawing the linework between widely spaced observations or where faulting is inferred from the interferometry but not field verified.

Portions of the cross fault that ruptured during the **M**6.4 earthquake had been mapped prior to the 2019 earthquake sequence, although at a small scale (1:250k) that lacked detail. The mapping is attributed to Hsu and Wagner (1990), unpublished, but was compiled by CGS for the most recent version of the USGS Quaternary Fault Database (USGS/CGS 2019). Traces that were mapped appear to be unnamed. Portions of the fault that ruptured during the **M**7.1 earthquake were mapped prior to the earthquake and appear to be located mostly NW of the intersection between the two ruptures. It appears these traces were unnamed as well. We are not aware of any maps that depict Quaternary activity on the part of the **M**7.1 rupture southeast of the intersection between the two faults.

For this report and as shown in Figure 2, we refer to the fault that produced the **M**7.1 rupture as the "East Little Lake Fault Zone" for parts NW of the intersection and the "South Little Lake Fault Zone" for the part south of the intersection. The fault producing the **M**6.4 fault is near the "Salt Wells Valley" but no name has yet been assigned; we refer to it as a "cross fault".

Separate reconnaissance activities occurred inside and south of the NAWSCL (approximately north and south of Highway 178). Within the base ground mapping and helicopter overflights were conducted primarily by USGS and CGS personnel escorted by US Naval personnel. South of the base, GEER performed detailed fault mapping and UAV flights.

Surface Fault Rupture Mapping North of Highway 178

July 4 2019 **M**6.4 Event

On the evening of July 4 2019, Janis Hernandez (CGS), Kelly Blake (US Navy), and Ken Hudnut (USGS) arrived at the Highway 178 crossing of the cross fault rupture. Prior to their visit, a 165 m wide zone containing four distinct fractures and several minor cracks was found to have N80E ± 2 degrees orientation where rupture crossed the highway. The team was joined by Ben Brooks (USGS) and others. Between the two teams working independently to estimate total displacement across the zone, an estimate of 40-50 cm of left-lateral offset was obtained. On one strand of this fault zone, the white painted stripe on the south side of Hwy. 178 was offset by 8.9 cm (see Fig. 3).

The overall trend of the zone was not clearly determined at that time (due to darkness). Hernandez followed some of the fractures out towards the southwest prior to night fall, but most of the observations made were on the Hwy. 178 asphalt and on the adjacent pipe that was being excavated by a crew in order to help repair the water pipeline that services Trona (Sec 2.2).

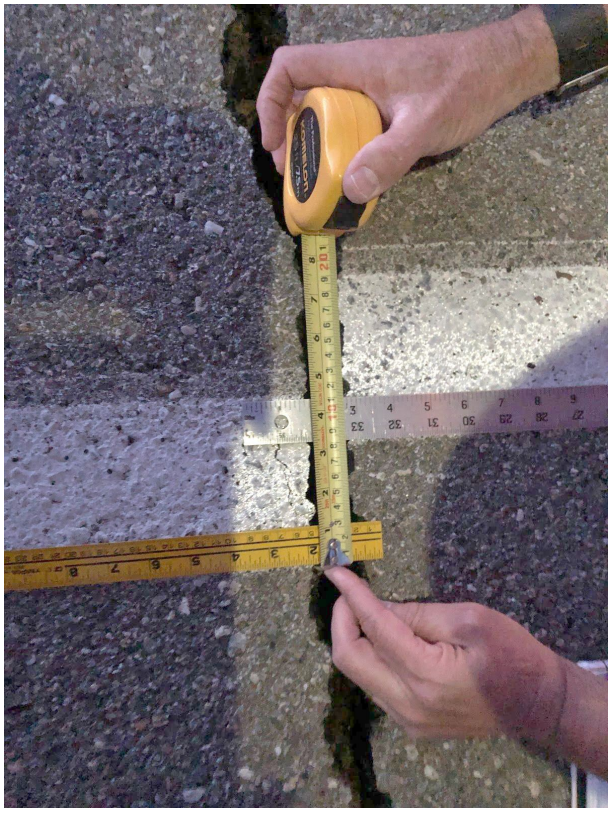

Figure 3. Measuring a fault offset on Highway 178 following the **M**6.4 earthquake on July 4, 2019. (Credit: Kelly Blake, US Navy. Public domain). Here, the fault breaks crossed the highway nearly perpendicular to the orientation of the highway, probably because the road surface was relatively strong and was easily able to de-couple from the road bed. The overall orientation of the fault zone at this site is about N 50 E (see Fig. 2) but the fractures crossing the road were measured at N 80 E (Lat./Long. 35.6442, -117.5356).

On July 5 in the morning, ground reconnaissance was conducted in the NAWSCL. The teams approached the epicentral area from the southwest to examine previously mapped strands of the Little Lake Fault Zone. Very little evidence of surface faulting was discovered during this ground reconnaissance. That afternoon, an aerial reconnaissance was supported by the California Highway Patrol. Janis Hernandez and Ken Hudnut conducted aerial reconnaissance of the entire cross fault rupture and collected stereo overlapped photographs using a Nikon D800 with GP1 and collected waypoints with a CGS data collector. Notably, upon examination of NW-to-SE oriented bedrock faults in the epicentral area, no cracking or rupture was observed. Numerous faults were clearly evident in the bedrock geology and where these were observed from the air, no cracks were present. GPS waypoints were collected along the flight tracks and this negative observation will later be scrutinized. In general, however, Hernandez and Hudnut

concluded at the time that the **M**6.4 surface fault rupture was entirely associated with the NE-to-SW oriented cross fault.

From the epicenter of the **M**6.4 event, the NE to SW oriented fault zone may be described as follows (see Figure 2 blue lines):

- From the NE end of the fault, the rupture is characterized by minor offsets across the break in slope, along the northwest side of a NE-SW-oriented ridge, along which a prominent set of NW-SE-oriented dikes is visible in satellite imagery (CGS FID 1022-1010) over a length of about 1.9 km where an access road is encountered.
- Moving further to the SW, the fault rupture jumps 0.8 km to the southeast. Another strand continues from USGS FID 836 and CGS FID 652, continuing 2.5 km SW across a range access road towards Salt Wash Valley. At the NE edge of Salt Wash Valley, the rupture crosses the point that was later ruptured through by the **M**7.1 earthquake. This is referred to as "the intersection" between USGS FID 828 and USGS FID 830. We are carefully checking airphotos and performing ground surveys to see if ruptures from the **M**6.4 were offset by ruptures from the **M**7.1.
- In the **M**6.4 earthquake, the rupture continued to the SW, crossing Salt Wash Valley for 1.7 km. In this section of the cross fault rupture, the rupture passed into water saturated fine-grained channel deposits. Along a portion of the rupture, where it crosses Salt Wash, sand boils were noted and photographed from the air near CGS FID 1016.
- The rupture then passes out of Salt Wash Valley and up into firmer soils (CGS FID 612). The distance from the intersection to CGS FID 612 is 1.7 km.
- From CGS FID 612, the rupture continues towards the SW for an additional 1.8 km to Highway 178.

The photograph in Figure 4, and photographs on the NAWSCL in subsequent figures, are provided without latitudes and longitudes. Due to Navy policy related to operational security considerations, geodetic coordinates of photographs in the base are not being published at this time.

July 5 2019 **M**7.1 Event

The first observation of surface rupture from this event was made by Ben Brooks and his team on the evening of July 5 at the mainshock rupture fault crossing of Highway 178.

On the morning of July 6, aerial and ground based teams began to map the rupture. For the next seven days, a team that averaged 14 geologists, escorted by Navy personnel, performed reconnaissance and documented the extent of the rupture (red lines in Figure 2) within the base.

Starting at the **M**7.1 epicenter (approximately at USGS FID 978), which is located approximately 3.5 km SE from the intersection of the boundary lines for Inyo, San Bernardino, and Kern Counties, we first proceed to the NW as follows:

- The rupture crosses the line from San Bernardino to Inyo County as it splays across a roughly 2 km-wide closed depression (USGS FID 883 and CGS FID 549). Significant rupture is observed on both sides of the topographic depression.
- Within Inyo County, rupture progressed for 2.5 km to the location shown in Figure 4 and then an additional 2.5 km further towards the NW on these two parallel fractures. These fractures then coalesced into one (USGS FID 763 to 1511) with minor fractures observed on the hillside immediately SW of the main break (e.g., USGS FID 790 to 1669).

a) **b)**

Figure 4. (**a**) Fault scarp located about 2.5 km north of **M**7.1 epicenter exhibits down to west separation and a small graben in the near field (view to North). The graben appeared to have been filled with water soon after the earthquake, as scour patterns and silt deposits issued out from the western lip of the graben and bathtub rings were preserved on the inside walls. Field book for scale. Nearby fault offset is 2.6 m (+/-0.5) horizontal, 0.55 m (+/- 0.2) vertical. (**b**) Liquefaction vents along trend a few meters east of fault scarp in left photo. (USGS photoby Kate Scharer)

- The rupture then began to splay and step on NE-to-SW oriented fractures with an overall dominantly left-lateral sense slip (USGS FID 1682 to 762). At this point one strand of the rupture crossed a dirt road called “Fae to Airport Lake road” as it crosses a closed topographic depression. One strand of the rupture continued along the NE edge of the White Hills, but the main break steps across the closed depression.
- Other large NW-to-SE oriented zones of cracks were observed at the SE edge of Airport lake (a playa) and 1.75 km from the edge of the playa (e.g., CGS FID 64 to USGS FID 898, USGS FID 919 to CGS FID 158, and USGS FID 862 to CGS FID 69). Additionally a NW-to-SE oriented fracture runs along the NE side of the Airport Lake closed topographic depression (CGS FID 1023 to USGS FID 864).
- Finally, one N-S oriented fracture passed from CGS FID 1031 to CGS FID 0 E-NE of the Airport Lake Playa.
- The distance from the epicenter to the NW end of the rupture is 17.5 km. Overall this NW limb of the rupture is characterized by right-lateral strike slip faulting, but near the NW end it transitions to NE-to-SW oriented faults with both strike-slip and local vertical separation components of slip.

Returning to the epicentral area (USGS FID 978) and moving SE, rupture propagated 32 km to the SE extreme end (well outside the base).

- From the epicenter towards the SE the rupture splayed with the eastern branch passing to the NE of China Lake (USGS FID 842 to CGS FID 280). The main strand passed directly through China Lake (a playa).
- From the epicenter towards China Lake, offsets increased dramatically and on the main strand the rupture pivoted slightly towards the south, creating a notable east side up vertical escarpment, where it passed two dirt roads (USGS FID 931) (Figure 5). This feature occurred only 350 m west of the USGS re-located epicenter of the **M**7.1 mainshock (USGS FID 931). Right-lateral offset at this location is about 3.4 m and the vertical separation is perhaps as large as 2 m. Some pre-existing topography, possibly indicative of a pre-existing fault scarp along this section of the fault (perhaps associated with prior fault slip), may have been present, contributing to the observed height of the fault scarp seen after the earthquake. This remains under investigation.

Figure 5. All six people are standing on a surface that was nearly flat prior to the **M**7.1 earthquake, and here the fault rupture offset the ground surface vertically by one to two meters, forming a fault scarp. The lateral offset of about 3 to 4 m shifted a dirt road set of tracks to the right (see Fig. 9 for additional details at this site). On each of the sides of the fault, three people are marking the same three features that have been offset; the center line of the road and each of the tire tracks. All are pointing to indicate the tectonic sense of right-lateral fault motion. (Credit; Photo by John Foster, US Navy; public domain).

- Both major splays of the rupture cross the major NS base access road and disrupted the pavement. The main strand of the rupture then enters the playa at its NW edge at CGS FID 585. From the NW side of the playa to the SE side of the playa, the main rupture continues for 3.5 km and it is over this section of the rupture that the largest surface displacements were observed. Within the NW edge of the China Lake playa, 0.6 km to the SE of CGS FID 585, we encounter offsets of 3.75 +/- 0.2 m (USGS FID 975). Further along by 0.7 km, we encounter 4.2 +/- 0.10 m offset (USGS FID 875), which is the maximum observed slip (Figure 6).

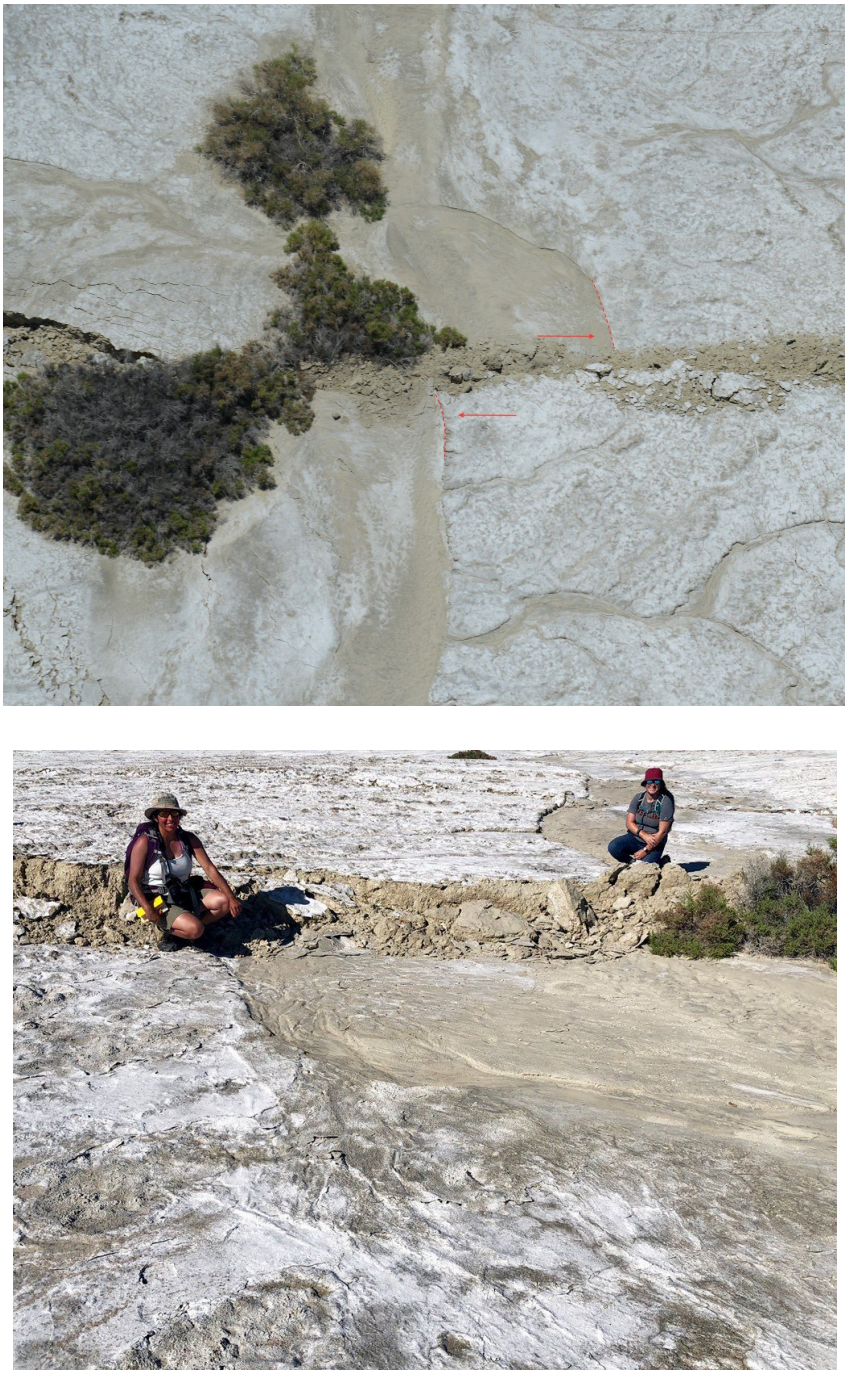

Figure 6. (a) Aerial and (b) ground view of a 4.20 m right-lateral offset on the dry China Lake bed. In Part (b) the offset is measured by Belle Philobosian (USGS) and Kelly Blake (NAWSCL Geothermal Program Office). Photographer in (b) was at the upper right of the photo in (a). The channel margin sharply demarcates the salt-crusted white surface of the pre-incisional dry lake bed surface from the fresh fine-grained deposits in the wide flat channel thalweg. This feature provides a reference allowing measurement of a displacement vector with small errors (approx. ± 10 cm). This is considered the maximum offset measurement (Credits: (a) Ken Hudnut, USGS, public release; (b) Brian Olson, CGS).

- The strand continues to USGS FID 874. At a small compressional step over, coincident with a small pre-existing hill (the existence of which may indicate prior ruptures across the playa), the rupture continues from USGS FID 960 to 2439, whereupon the rupture exits the playa and continues to the SE.
- A prominent power line that runs EW across the southern margin of the playa is offset 2.7 m right laterally, based on field mapping and later confirmed by truck-mounted lidar (Figure 7) The width of the fault rupture zone near the power lines, measured as the maximum distance between ground cracks observed perpendicular to the fault in this area, is approximately 320 m. Interestingly, a few hundred meters north of this location, the main fault strand narrows to only a few meters.
- To review and summarize rupture across the playa, from the epicenter to the SE edge of the playa (USGS FID 2439) is a distance of 7 km.
- From this point, the rupture passes back into sandy soil for 0.8 km where the rupture encounters and offsets an asphalt base access road. Measured offset at this location was 2.5 m ± 0.2 m right lateral with a localized vertical separation (east side up) (USGS FID 2419) (Figure 8). The fault zone width in this area was measured as approximately 80 m based on locations of asphalt cracks.

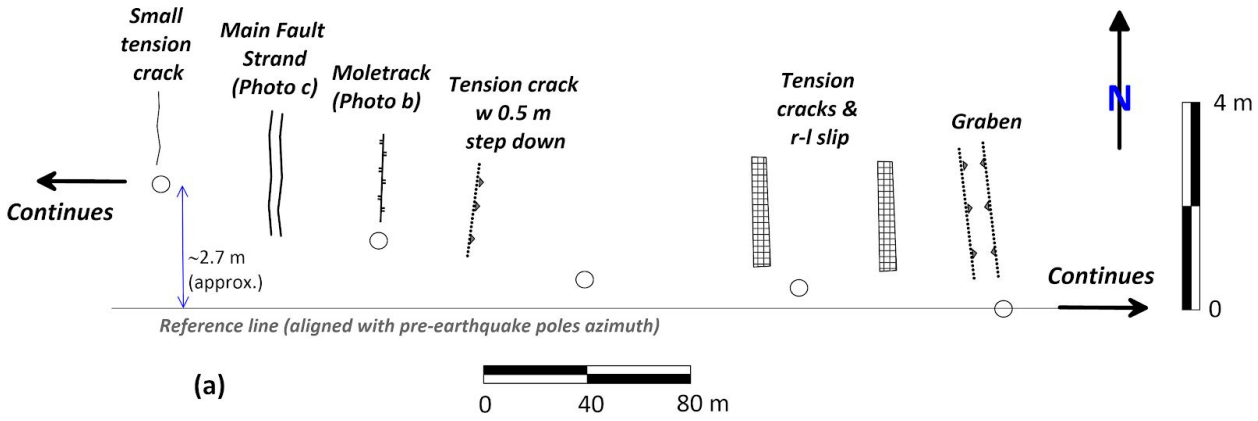

(b)

(c)

Figure 7. (a) Field mapping of line of power poles offset by surface rupture near the southern margin of the playa and ground deformations in dirt road immediately north of poles. The mapping indicates features over the full width of the fault zone. The utility pole locations are approximate from field mapping; more accurate surveying has been undertaken by USGS and will be published separately. (b) Moletrack photo at location labeled on map. (c) Photo of main strand near road crossing.

Figure 8. Helicopter overflight viewing access road fault offset. The CGS and USGS, along with National Guard and Navy personnel, view road damage showing 2.5 +/- 0.2 m of right-lateral motion along the primary rupture associated with the magnitude 7.1 event. This offset access road was broken by the mainshock fault rupture about 800 m southeast of the China Lake playa (Credit: Ken Hudnut, USGS. Public domain)

- Proceeding SE from the access road shown in Fig. 8 by 0.16 km, the rupture then encountered an abandoned railroad line between USGS FID 872 and 967. The railroad bed has been offset 1.8 m right-laterally. The pattern of rupture in the railroad ballast fill was mapped as shown in Figure 9, with an approximate width of 30 m

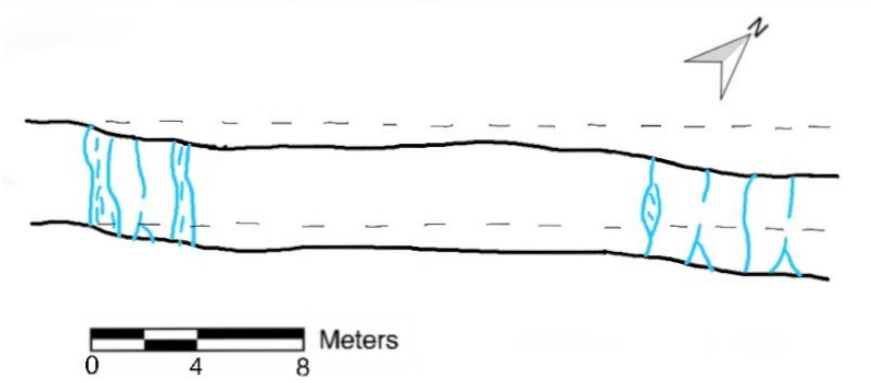

Figure 9. Map of railroad embankment with cumulative offset of 1.8 m. The embankement is of offset on two distinct strands of the fault, with an overall width of the rupture zone of about 30 m.

- From this point to the SE, the rupture enters low hills where the fault is clearly offsetting two differing types of bedrock on the NE and SW sides. In the bedrock, and the shallow soil on the edge of the hills to the south, the fault zone width decreased to a few meters, which represents considerable narrowing relative to the 30 and 80 m widths mapped in thicker soils to the south.
- The rupture continues for a distance of 3.9 km along a SW-facing hillside that is characterized by multiple sub-parallel drainages that we refer to as “offset gullies” (Figure 10). A hillside bench was formed along this same NW-to-SE oriented ridge, down to CGS FID 1053 to 1051. At the offset channel locality at CGS FID 1051, Janis Hernandez (CGS) made a set of detailed observations on July 8, 2019. She found offsets of less than one meter.

Figure 10. A series of nearly parallel and sharply incised small drainage gullies occur along a NW-SE oriented ridge line that lies from 1 km to 3 km southeast of the offset access road shown in Fig. 8. The roughly twenty such gullies shown in this photo are referred to as the “offset gullies”. The short dashed red line segments indicate the location of the mainshock fault surface rupture, which forms a bench as the fault cuts across this hillside, nearly perpendicular to these gullies. With high-resolution topography from the air photos already collected, and potentially from the airborne lidar in the future, geologists expect to be able to precisely measure fault slip variation along this section of the fault. Slip is known to diminish from approx. 1.8 m at the abandoned railroad tracks down to less than one meter at the SE end of the ridge where these gullies were found. So, it is expected that these gullies will afford a way to quantify the reduction in slip from NW to SE along this 2 km long section of the fault.

- From CGS FID 1051 the rupture continued for 3.75 km to “the intersection” with the **M** 6.4 cross fault. It then continued paralleling the NE margin of Salt Wells Valley for 1.95 km. The main fault rupture then crossed Salt Wells Valley between USGS FID 818 and 2486. Approximately 100 m south of the wash, the fault offset a chain link fence with a right-lateral sense of motion, approximately 45 meters north of Highway 178 (Figure 11). The main rupture then crossed Highway 178 at UNR FID 1378.
- The distance from the epicenter to the fault crossing at Highway 178 is 19 km.

Figure 11. Offset fence line at southern Salt Wells Valley, just north of highway 178. The fence offset is 70 ± 5 cm right-lateral sense. (photo by Jason R. Patton, CGS; Lat./Long. 35.6495, -117.4828)

Detailed displacement vectors are being developed by a variety of methods at this time. As one example, Figure 12 shows the use of relatively high-accuracy (few cm) GPS to document the 3D displacement vector for a locality with a broad zone of distributed faulting where a dirt road crosses the rupture (a transtensional stepover zone about two kilometers southeast of the relocated epicenter). At this site, also shown in Fig. 5, the escarpment that formed along the

fault expresses the greatest amount of vertical separation along the entire mainshock rupture. Because the fault zone is relatively wide at this site, and may have a pre-existing scarp and gully along where the new scarp formed in 2019, it presents a special challenge for accurately observing the fault displacement. As shown in Fig. 10, the GPS was therefore used to quantitatively address the total offset at this site, and its lateral and vertical components.

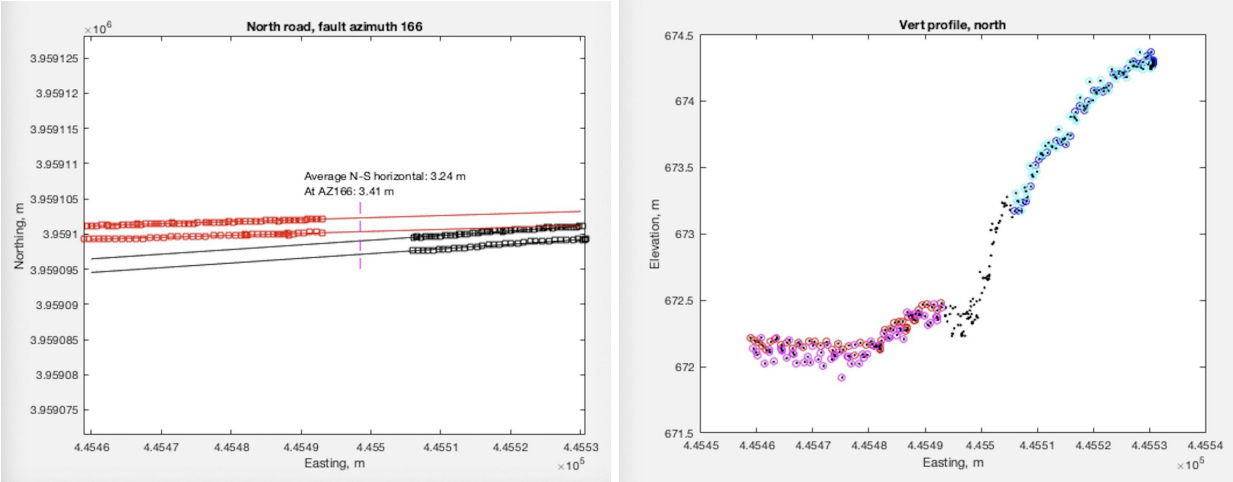

a) **b)**

Figure 12. a & b. A handheld high-accuracy GPS unit was used to measure points along the dirt road that is shown in Fig. 5. The dirt road tire tracks extending out in either direction from the fault offset were measured to within a few cm's accuracy at hundreds of points. These lines were then used to estimate the fault offset more accurately than could be done using conventional methods such as with a tape measure and straight-edge rulers (as in Fig. 3). In this location, extensive cracking was seen across a width that extended more than 350 m to the west of the scarp, and over 150 m east of the scarp, for a total width of more than 500 m at this location. The dirt road azimuth was estimated by GPS to be 166 degrees, and the fault rupture trace was projected so as to estimate that fault offset was 3.4 m right-lateral in the plane of the fault (panel a). Over two meters of vertical separation was also quantified by GPS at this location (panel b), but half of this may be a pre-existing channel, perhaps apparent offset along what could be a scarp formed in a pre-historic earthquake The pre-existing topography at this site is still being discussed and debated as a possible contributor to the apparent 2 meter scarp height here.

Post-mainshock afterslip monitoring has been undertaken using different methods. At Highway 178, lines were painted across ruptures in the asphalt surface to enable checking of subsequent slip (Figure 13). These lines were painted onto the pavement shortly after the **M**6.4 and **M**7.1 mainshocks; no afterslip was observed through July 8 2019. GPS monitoring in the region is ongoing. Satellite based monitoring of afterslip is occurring more broadly along the fault, with some evidence of afterslip having been encountered in China Lake.

Figure 13. Pavement of Highway 178 offset by **M**6.4 event fault rupture (shown by white lines) and short painted lines used to monitor afterslip. Locations: Left 35.649, -117.4824 (red line), Right 35.6441, -117.537 (white line). Photo credits: Ben Brooks, USGS

Mapping South of Naval Base - Overview

Between July 5 and 8, geologists from the University of Nevada, Reno (UNR), Arizona State University (ASU), California State University, Fullerton (CSUF), and the CGS inspected the surface fault rupture traces of both the **M**6.4 and **M**7.1 ruptures on foot. Surface rupture locations were documented by GPS and observations on the character of the rupture, types of faulted deposits, amounts of displacement, and other parameters were recorded. Observations along both ruptures extended from Highway 178 to the approximate southern termination of each rupture for distances of ~5 miles (~8 km) and 8 miles (~13 km) along the **M**6.4 and **M**7.1 ruptures, respectively.

South of the Highway, the **M**6.4 rupture extends southwest along the southeastern side of a low linear bedrock cored ridge where it is characterized by distributed zones of right stepping en echelon fissures and moletracks, anastomosing surface cracks, and left-lateral offsets of subtle gullies and drainage swales (Figure 14). Although the primary rupture was along the southeast side of the ridge, distributed cracking was observed along the crest of the ridge and

along its northwestern side suggesting that the ridge is the product of progressive tectonic deformation. Southwest of the ridge, the rupture continues as a complex pattern of right-stepping en echelon surface cracks and fissures that cut across alluvial fan and wash deposits. Towards the southwestern termination of the rupture the distance between individual right steps becomes longer and surface cracks become tighter and more sinuous. The largest surface fissures along the **M**6.4 rupture are up to 90 cm wide and 50 cm deep, however the majority of the fissures on the order of 5 to 20 cm wide and deep. Along the length of the rupture the zone of deformation ranges in width from about 45 to up to 300 meters wide. Direct piercing points are rare along the rupture trace due to the subtle topography and diffuse margins of geomorphic features and dirt roads. However, left lateral offsets were measured at several locations and range between 37 and 60 cm (Figure 15). Overall, the character of the rupture was consistent and exhibited similar surficial expression along the length of the rupture investigated.

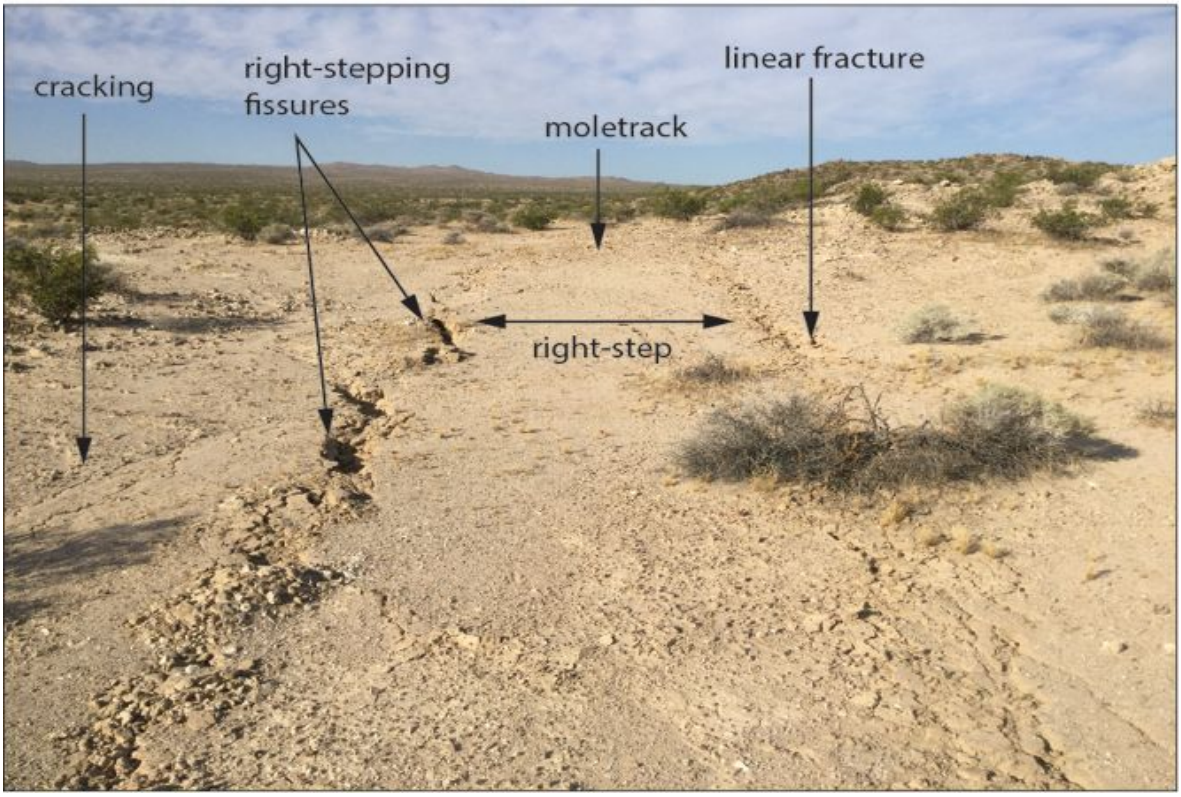

Figure 14. Typical right-stepping and overlapping surface cracks generated by the **M**6.4 rupture southwest of Highway 178. View to southwest. (Lat./Long. 35.6413, -117.5391). Photo credit: Rich Koehler.

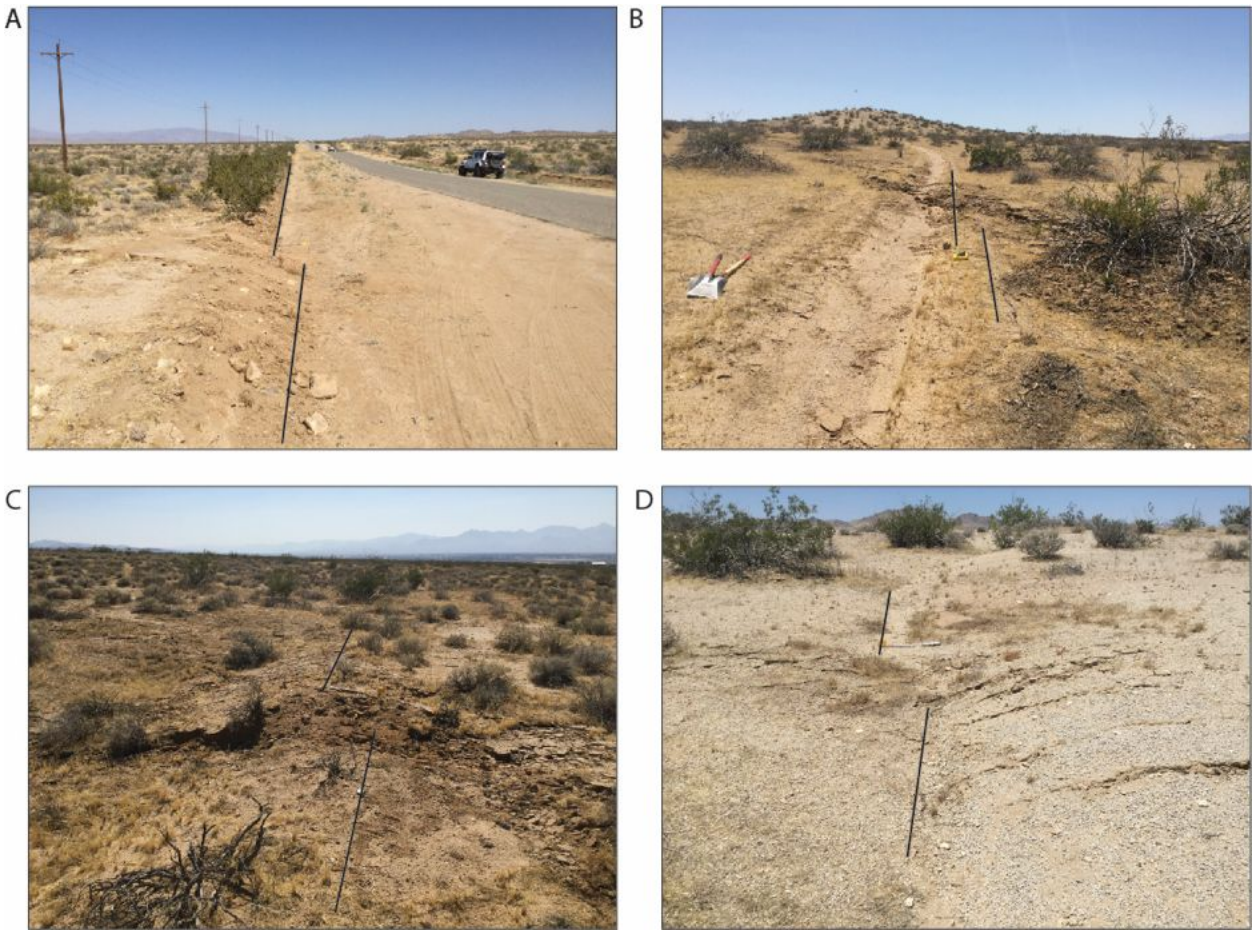

Figure 15. Observed left-lateral offsets along the **M**6.4 rupture (black lines) including (A) 60 cm displacement of Randsburg Wash road, view east (Lat./Long. 35.6178, -117.5734), (B) 37 cm displacement of a motorcycle track along a dirt road, view west (Lat./Long. 35.6312, -117.5563), (C) 60 cm displacement of the crest of an erosional swale, view northwest (Lat./Long. 35.6155, -117.5758), and (D) 45 cm displacement of a wash gully, view northwest (Lat./Long. 35.6336, -117.5522). Photo credit: Rich Koehler.

The **M**7.1 rupture extends 8 miles (~13 km) southeast from Highway 178, across the crest of the Spangler Hills to the Searles Lake basin. Within the Spangler Hills, the rupture is expressed as left-stepping en echelon surface fractures and fissures separated by small moletracks where it cuts across bedrock surfaces with thin lacustrine and soil cover, and remnant tufa deposits from paleo lake Searles (Figure 16). In this area, fissures are typically <10 cm wide and deep, however the largest fissures are up to 30 cm wide and deep. Moletrack scarps are typically 10-15 cm high, ~1 m wide, and characterized by cracked blocks of duricrust soil. A number of gullies are offset by the rupture up to ~1 m within the Spangler Hills. Distributed cracking occurs over a width of at least 100 m. Southeast of the crest of the Spangler Hills the rupture is characterized by down-to-the-southwest vertical scarps up to 70 cm high and right lateral

offsets of colluvial boulder rubble swales from 70 cm to up to 1 m where it extends across saddles and southwest facing bedrock/colluvial slopes (Figure 16).

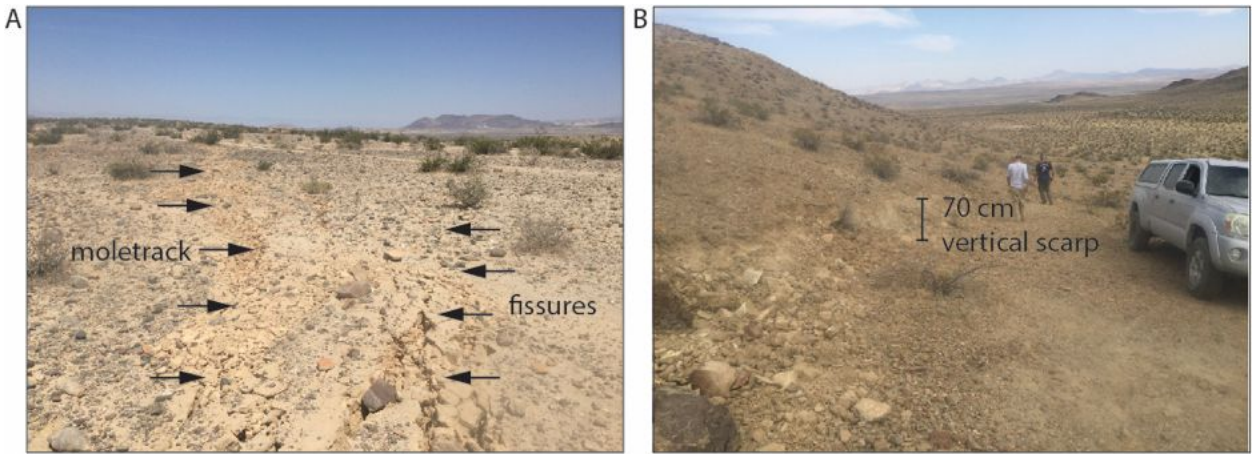

Figure 16. (A) Left-stepping fissures and moletracks (Lat./Long. 35.6380, -117. 4546), and (B) vertical scarp (Lat./Long. 35.6217, -117.4277) within the Spangler Hills. Photo credit: Rich Koehler

From the southeastern flank of the Spangler Hills, the fault extends down the axis of a broad active alluvial fan to the vicinity of the Trona railroad alignment. In this area, the rupture continues in a left-stepping en echelon pattern of fissures and moletracks with the largest fissures up to 60 cm wide and 30 cm deep (Figure 17). Right-lateral offsets of several drainage gullies and dirt roads were observed to have a total displacement of up to 1 m (Figure 17) typically distributed across several subparallel strands across a 20-30 m wide zone. The rupture displaces the Trona rail alignment across the main trace and across a secondary trace about 1.5 km to the southwest. Deformation of the rail alignment includes right-lateral displacement of the rail bed, kinking of the tracks, and jostling of railroad spikes (Figure 18).

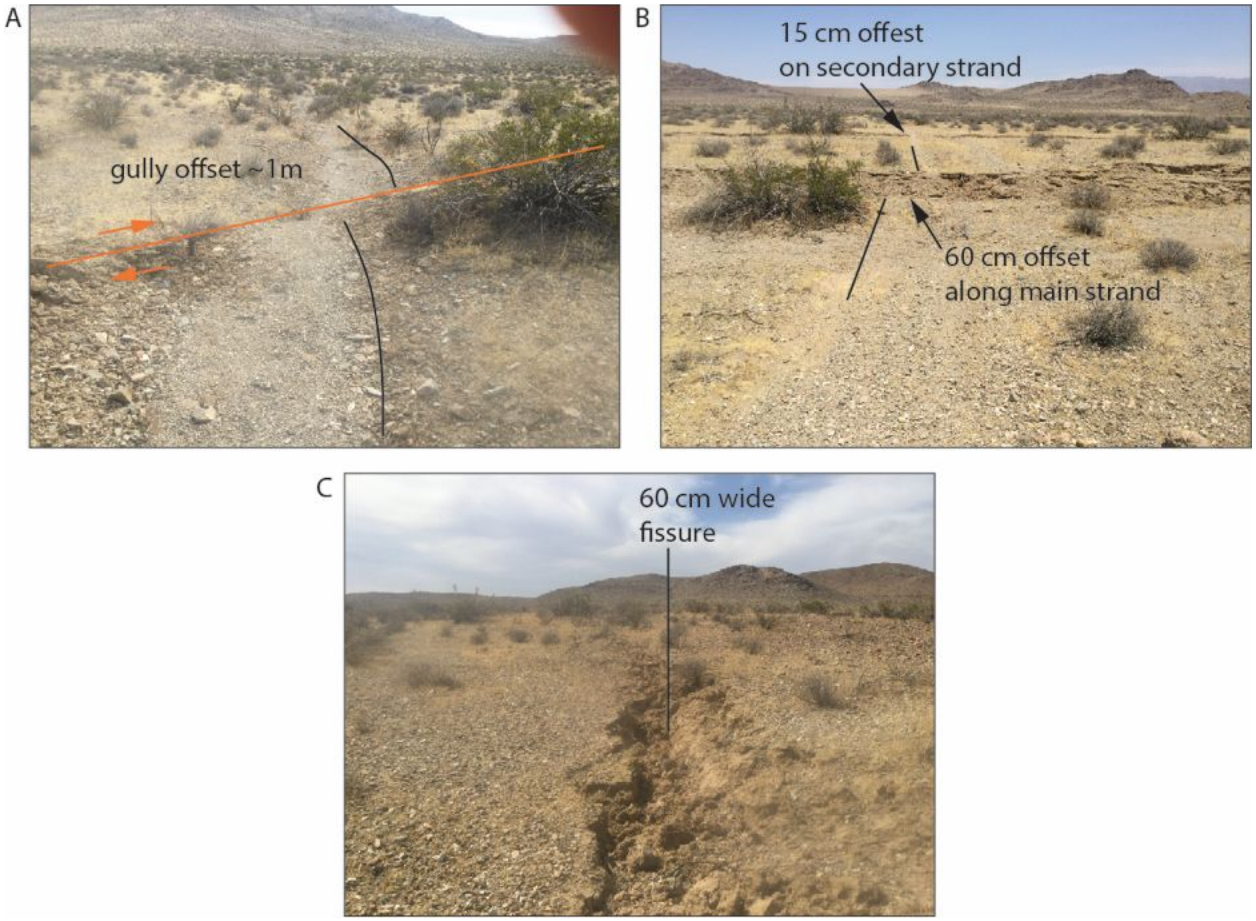

Figure 17. Photographs of the rupture where it cuts an alluvial fan on the southeast flank of the Spangler Hills including (A) ~1 m right-lateral offset of a gully (Lat./Long. 35.6172, -117.4236), (B) right-laterally offset dirt road, 60 cm across main strand and 15 cm across parallel subsidiary strand (Lat./Long. 35.6022, -117.4069), and (C) a large fissure (Lat./Long. 35.6171, -117.4227). Photo credit: Rich Koehler.

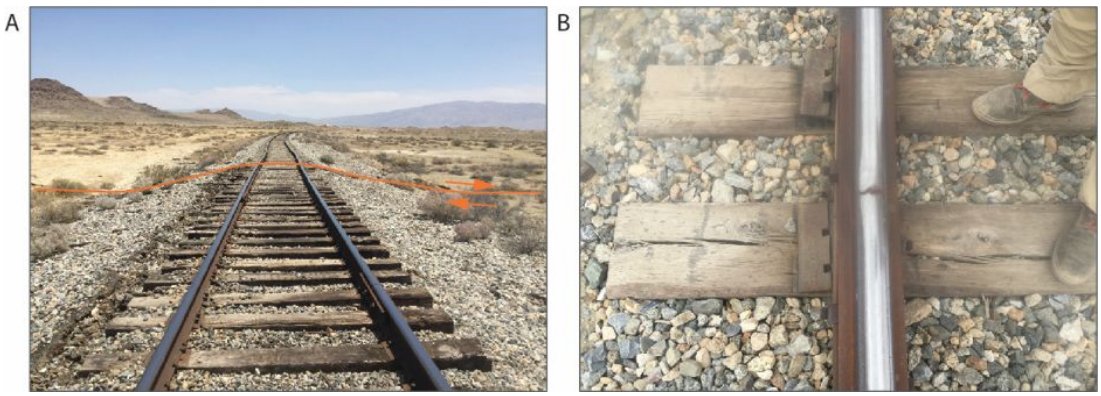

Figure 18. (A) Right-laterally offset rail bed and bent tracks along the main rupture trace (Lat./Long. 35.5944, -117.4004) and (B) kinked tracks and jostled rail spikes along a secondary trace (Lat./Long. 35.5872, -117.4141). Photo credit: Rich Koehler.

Southeast of the railroad tracks the fault extends southeast across lacustrine deposits of paleo Lake Searles for approximately 600 m before making a 50-70 m left step across an isolated low bedrock hill. In this area, rupture traces are confined to a 10-30 m wide zone and wash channel margins are displaced up to 1 m right-laterally and up to 40 cm vertically down to the southwest (Figure 19). Numerous closely spaced cracks extend across the bedrock hill. The presence of this hill within a left-step along the fault indicates persistent long term uplift within the step. Southeast of the bedrock hill, the rupture continues in a left-stepping en echelon pattern of fissures, moletracks, and small vertical scarps (~5-20 cm) across lacustrine deposits and numerous active washes to its southeastern termination. Distances between individual left-steps range from several meters to over 10 meters and lateral displacements of channel margins and dirt roads of 75 cm to 1 meter were observed (Figure 19).

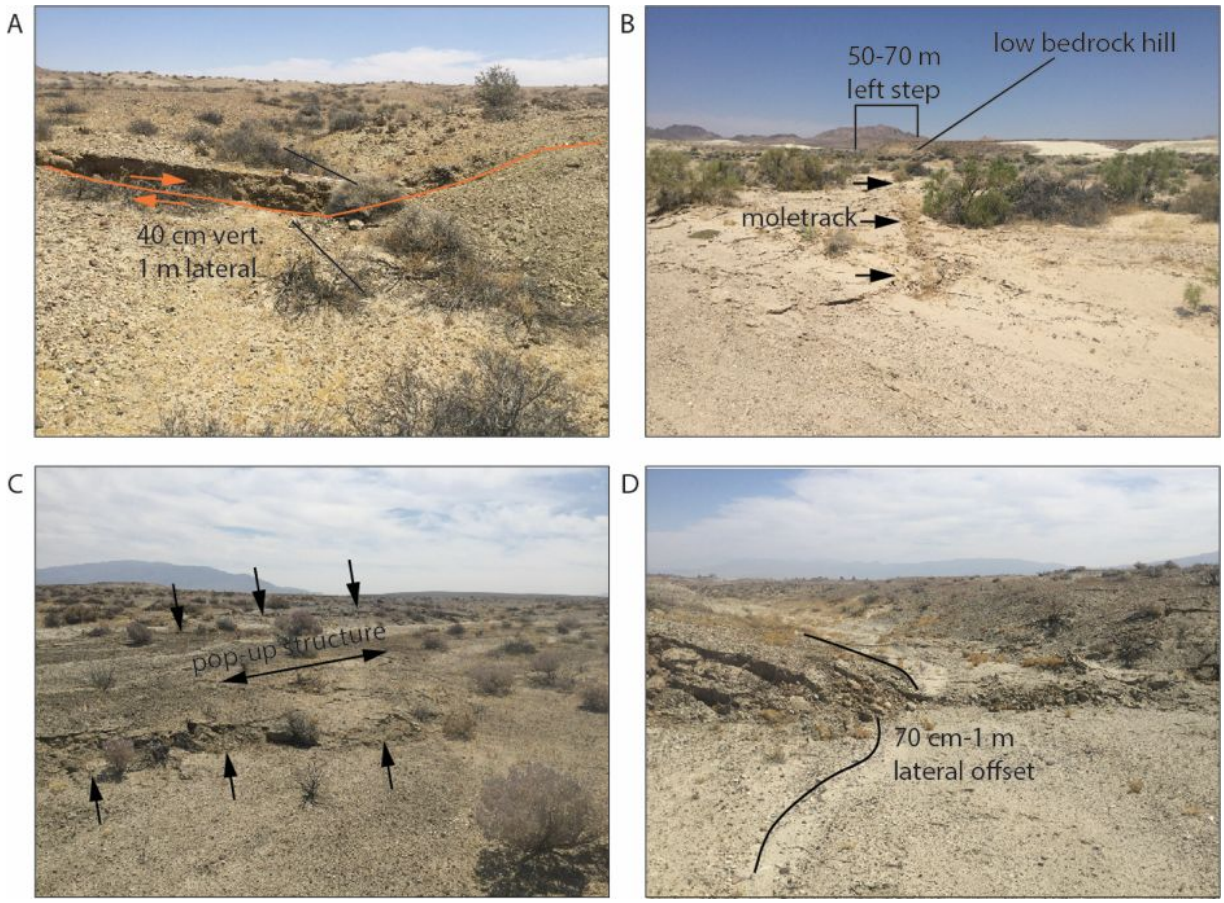

Figure 19. Photographs of the **M**7.1 rupture south of the Trona railway. (A) 1 m right lateral and 40 cm vertical displacement of small drainage, view northeast (Lat./Long. 35.5917, -117.3978), (B) moletrack projecting northwest into 50-70 m wide stepover in rupture trace (Lat./Long. 35.5869, -117.3903), (C) left stepping scarps in active wash connected by pop-up structure, view west (Lat./Long. 35.5856, -117.3889), and (D) right-laterally displaced channel margin (70 cm-1 m), floor of active wash displaced vertically up on NE about 30 cm, view NE (Lat./Long. 35.5826, -117.3845). Photo credit Rich Koehler.

The southern terminus of the **M**7.1 rupture is characterized by a chaotic mix of distributed extensional fractures ranging in orientation from north-south, northeast, and northwest that are distributed across a zone at least 1.6 km long and 1.2 km wide. Several prominent north-south oriented fractures extend in length for over 1 km. Surface breaks were not observed south of Searles Valley Road. The Garlock fault was investigated just to the south of its intersection with Randsburg Wash Road, and no evidence of surface rupture or cracking was observed.

Detailed Fault Mapping South of Naval Base

The USC- and UCLA-based GEER team mapped the two fault zones in the longitudinal direction south of Highway 178 and along several transects sub-parallel to the Highway. The team's strategy was to collect perishable information as quickly as possible, and to document the widths of cracks and distributed shear zones along with apparent horizontal and vertical offsets of the ground at specific locations. The soil in the fault areas is prone to disturbance from the horde of "earthquake tourists" visiting the site and is soft and dry enough to even be disturbed by wind action (Figure 20), hence early data collection was critical. The team used geolocated pictures from the native iPhone "Camera" app and the "Solocator" app along with tracks from the smartphone app "GPS Tracks" to document cracks and fault displacements. On some of the surveys, measuring tapes and surveyor sticks were included in the pictures to provide ground control measurements to be analyzed later in the lab. The areas covered by the team are relatively small, but are covered in detail. The purpose of this work is to create ground-truth measurements to correlate with the UAV structure from motion (SfM) digital elevation models in those areas and provide constraints on what is visible from this and other remote sensing methods applied in broader areas. Since the purpose is not to document the fault trace itself, but to develop constraints for remote sensing, we provide a general description of the observations and provide a summary of the data collected by various means.

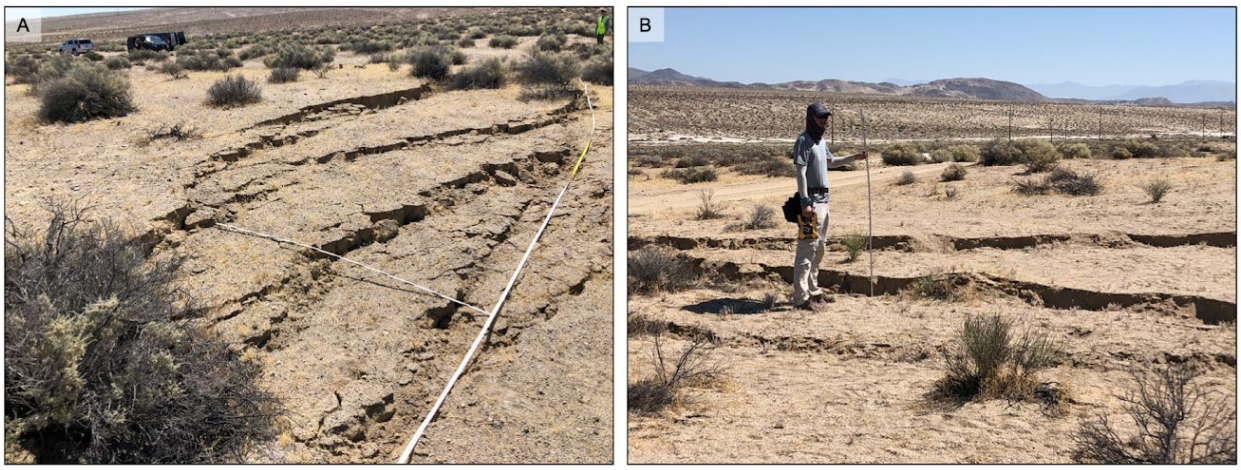

Figure 20. Photographs of the **M**7.1 rupture taken the day after the rupture, July 6 (A, 35.6470, -117.4801) and on July 11 (B, 35.6457, -117.4790). Photo A was taken just south of the dirt road, Photo B was taken just north; the fault traces generally exhibit similar features. Although not taken exactly at the same location, the two pictures illustrate the typical degradation of features from people visiting the site within a span of 4 days. Photos by Christine Goulet.

M7.1 fault trace; detailed mapping

For the fault trace from the **M**7.1 event, one team focused on documenting the two main strands of the fault from Highway 178 to the first dirt service road (B1 to the East and B2 to the West, Figure 21). At the north end near Highway 178, the strands mostly coincide. South of Highway 178, the zone remains relatively narrow, for example as shown in Figure 22 where the width is 3 m about a third of the way south of Highway 178 towards the service road. The strands diverge towards the service road, creating a localized extensional graben that is 60 m wide along line B5. The ground in the extension zone is about 40 cm lower relative to the zones outside of the fault strands. Line B1 followed the main eastern strand starting at Highway 178 and extended in a SE-direction for 1150 ft (350 m) and line B2 followed the second strand toward the south. Generally, longitudinal cracks appeared in the stiff upper crust of the arid alluvial soil, with openings ranging from a few mm to 50 cm right at the surface. Lateral offsets in that area are marginal and vertical offsets were observed up to 16 in (40 cm) in some locations (Figure 23). The fault crossing at the dirt service road near line B5 as shown in Figure 24.

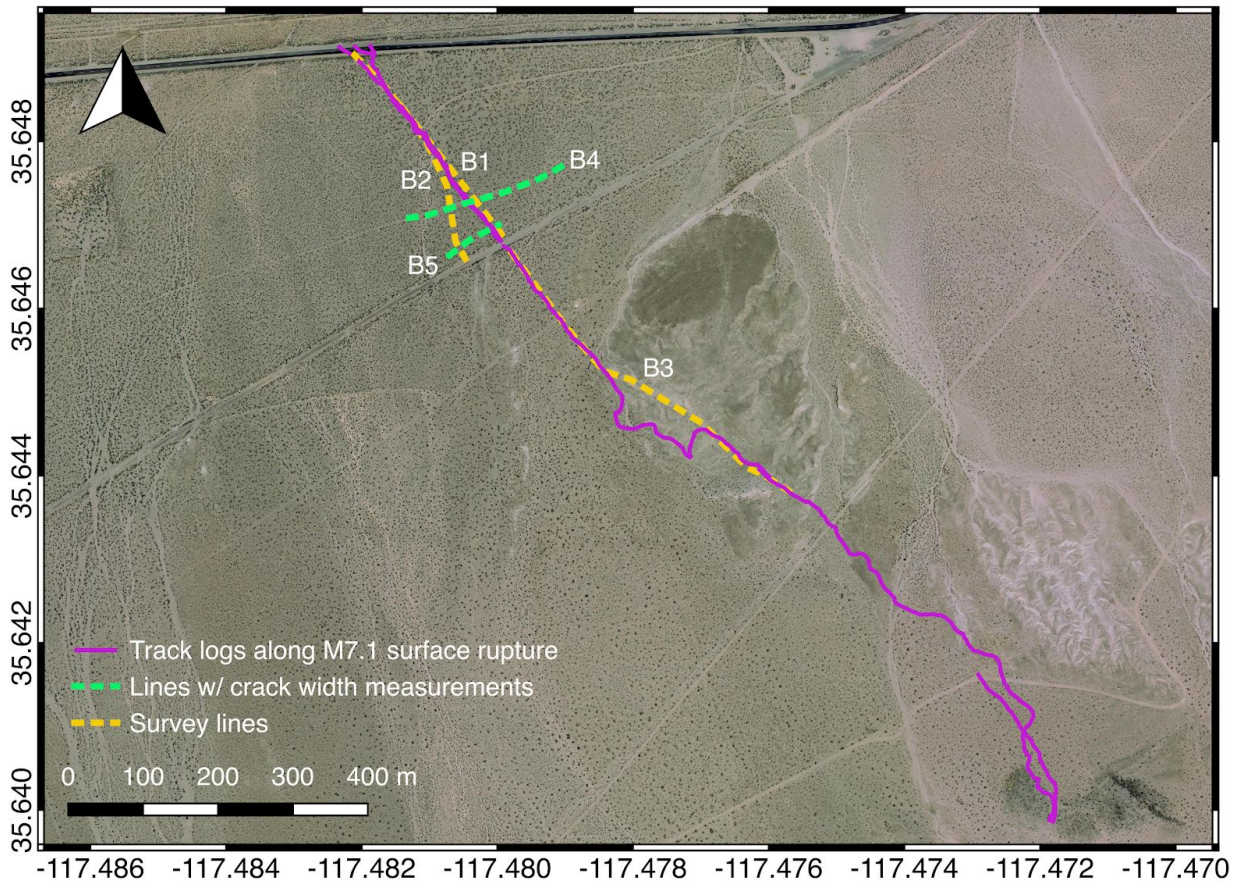

Figure 21. Fault trace mapping at location of the surface rupture from the **M**7.1 event just south of Highway 178.

Transects B4 and B5 were followed to capture the full fault zone width. We bound the transect end-points by walking several meters past the points shown on Figure 21 to ensure no cracks were visible beyond those points. On these transects, we took continuous and overlapping pictures of the fault zone following a measuring tape on the ground. The cracks' location and width data are to be quantified in the lab.

Figure 22. Fault rupture from the **M**7.1 event south of Highway 178 showing a 3 m band of concentrated deformation (35.6483, -117.4813). Photo credit Christine Goulet.

Figure 23. Fault rupture from the **M**7.1 event showing 40 cm of apparent vertical offset at a location approximately 146 m south of Highway 178 (35.6470, -117.4802). Photo credit Sean Ahdi.

Figure 24. Fault rupture from the **M**7.1 event showing at a road crossing south of Highway 178 (35.6468, -117.4800). Photo credit Scott Brandenberg.

The GEER team also recorded track logs along surface fault rupture traces using the "GPS Tracks" app. The track logs are shown in purple in Figure 21. These tracks generally follow the fault rupture zone, but they do not delineate individual ground cracks. The ground cracks were generally observed to be parallel to the track logs over much of the fault trace, though ground cracks transitioned to lie at approximately 45° angles from the fault strike toward the southeastern limit of the track.

Line B1 and the purple tracks shown on Figure 21 were mapped on July 6. Lines B2 and B5 were captured on July 7. Line B3 and B4 were documented on July 11. Line B4 outside of the main strands was not damaged by trampling and its intersection with features documented in lines B1 and B2 allows us to anchor the fault zone location.

M6.4 fault trace; detailed mapping

The process for performing detailed mapping along the **M**6.4 fault was similar to that described for the **M**7.1 trace. The study area extended from Highway 178 to approximately 300 m to the south. In that area, the fault zone appeared more diffuse than for the **M**7.1 fault, so detailed crack measurements along continuous longitudinal lines were not performed. Transects A1 and A2 were documented in detail so as to constrain the fault zone width, using continuous and overlapping pictures of the cracks along the extended measuring tape. As for the **M**7.1 fault, the limits of the transects were defined by the teams walking further SE and NW until no more deformations were visible. Two teams measured crack widths and documented their locations along transects A1 and A2 just south of Highway 178. Another team tracked continuous cracks using the "GPS Tracks" app as described above (purple lines on Figure 25). A separate track log was recorded for each surface rupture splay by starting the track log, walking along the surface rupture a distance of a few hundred meters on either side of Highway 178, then terminating the track log. This process was repeated for surface rupture splays over a width of a few hundred meters. We walked in a direction perpendicular to the fault strike about a hundred meters further in both the NW and SE directions, and did not encounter additional ground cracks. The surface rupture extended further toward the northeast and toward the southwest as this mapping effort focused on the region near Highway 178, and was conducted in parallel with an effort by other GEER team members to map the crack widths along transects perpendicular to the fault strike. The followed tracks are shown in purple in Figure 21. The purple lines do not represent all of the ground cracks, but the most obvious continuous ones. Additional cracks were observed along A1 and A2, which were documented on July 7.

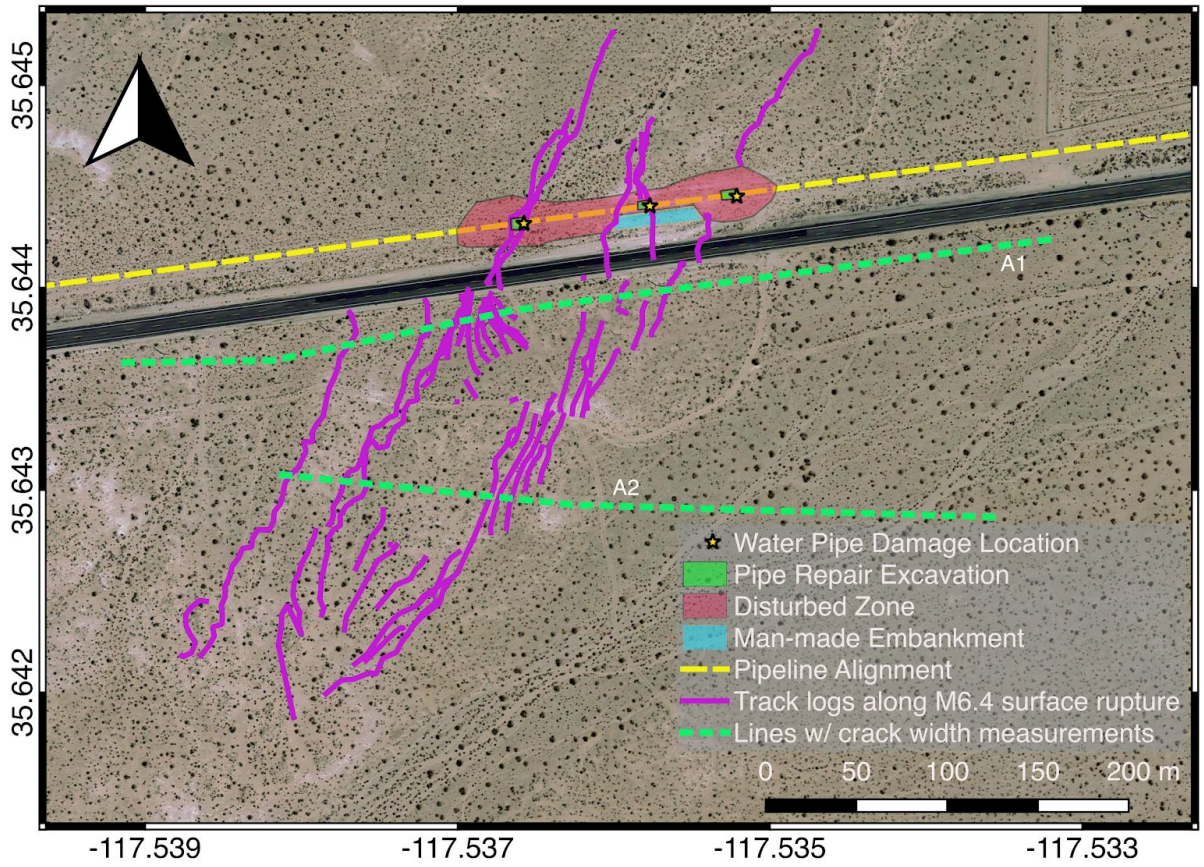

Figure 25. Fault trace mapping at location where surface rupture for **M**6.4 event crosses Highway 178. Map traces available in DesignSafe at Community Data / Main / Recon Portal / 2019 Ridgecrest, CA Earthquake / GEER Resources (see also Fig. 3 from this same location).

Additional Ground Deformations

We have documented additional ground deformations that appear to be fault strands located away from the main ruptures from the **M**6.4 and **M**7.1 events. These areas are shown on Figure 26. We have shared the location of those features with several groups, including the USGS and SCEC, so that future reconnaissance and remote sensing teams can add them to their investigation region.

The first displacement area (01 in Figure 26) was observed East of the **M**7.1 rupture and contained cracks parallel to the main rupture. The cracks appeared on Highway 178 following the **M**7.1 (they were not observed right after the **M**6.4 event), crossing it perpendicularly. The cracks were not continuous and we were only able to observe them up to roughly 50 m away from the road, on the north and south side. The observed cracks were fairly narrow and concentrated in a narrow area as well. The site was visited on July 7 and 11.

The other three zones of cracks were found crossing the Pinnacles Road, the dirt road leading to the Trona Pinnacles National Natural Landmark. These observations were made on July 12. The four areas showed persistent cracks generally trending from E to ENE to NE and were interspersed with variably trending set of secondary cracks (example on Figure 27). It is possible that some of the observed ground failure may be due to lateral spreading, however, we have not observed any sand boil or moisture in the cracked areas. The cracks were followed on the east and west sides of the road for about 60 m to 120 m on each side.

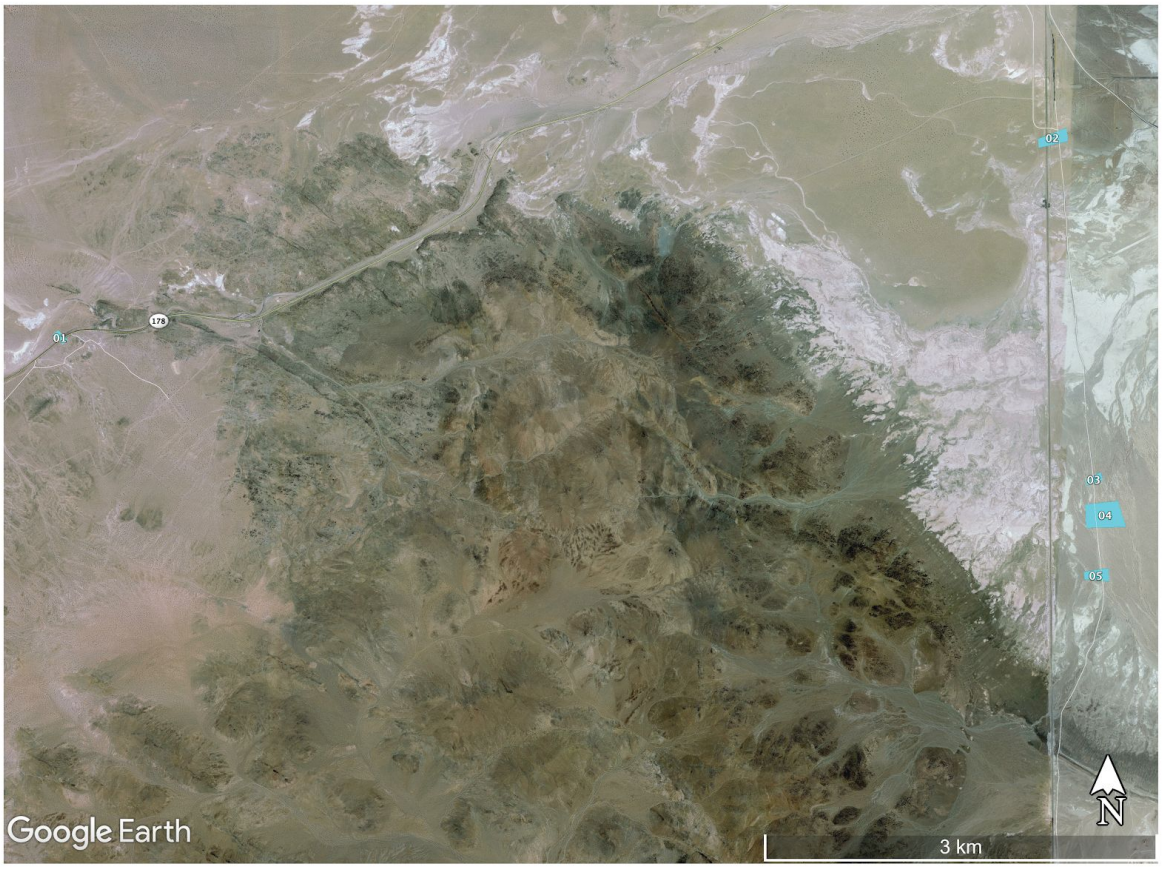

Figure 26. Map showing the different zones exhibiting cracks (numbered cyan polygons).

Figure 27. Example of cracks observed along Pinnacles Road. This specific picture was taken at zone 3 and shows where the cracks cut the Pinnacles Road.

2.2 Lifeline Performance

The most significant lifelines in the epicentral area support Ridgecrest, Trona, and the NAWSCL. In addition, the Los Angeles Department of Water and Power maintains significant infrastructure corridors to the west transmitting water and power from the Owens Valley area to Los Angeles. In this section we briefly describe performance of lifeline system infrastructure in the greater region around the Ridgecrest earthquakes gathered by July 12, 2019. Information on lifeline system performance in NAWSCL could not be obtained.

Highways and Roads

Caltrans maintains a system of state highways and Kern and San Bernardino Counties maintain county highways in the region. There were no reported damages to bridges. Highway 178 passing between Ridgecrest and Trona was damaged by fault offset up to a meter in several locations. There were also transverse cracks in highways and roads near the main fault rupture, but the cause is not yet defined. Other paved and unpaved roads in the desert were also offset by fault rupture. Some local roads in Trona had pavement damaged from lateral spreading. Highway 178 was temporarily shut down between Ridgecrest and Trona until cold patch was placed over the cracks, but remained in use following the patching. Repairs for fault rupture initiated on July 7, 2019 and proceeded with one lane alternating in service requiring a traffic escort. A few streets in Trona were blocked off from use due to compression bulging from lateral spreading.

Several state highway routes were impacted by rockfalls from the July 5 event. Highway 178 in Kern Canyon, more than 50 miles west of epicentral area, experienced a rock fall and was

temporarily shut down in Kern Canyon until the rock debris was safely removed. Highway 178 in Kern Canyon was reopened on July 6, 2019. Highway 190 near Townes Pass and Highway 127 near the Tecopa Hot Springs turnoff experienced some rock fall, which were cleared by 11:42pm July 5, 2019 (Twitter, Caltrans District 9@Caltrans9). US395 had large boulders fall onto roadway, which were cleared within a few hours (Mosalam 2019).

Railroads

A railroad parallels Pinnacles Road, near the southern end of the rupture from the **M**7.1 event. It was displaced right laterally, as described further in Section 2.1.

Water Systems

The Indian Wells Valley Water District (IWVWD) provides water service for Ridgecrest. Initial reports from IWVWD identified no pipe repairs from either earthquake, some repairs to air-vacuum valves, and small leaks in two tanks (one bolted and one welded steel tank).

The Searles Domestic Water Company (SDWC) provides water service for Trona. SDWC obtains supply from groundwater west of Trona, extending into the Ridgecrest area and the NAWSCL, and conveys it to the town in two supply pipelines. One supply pipeline runs roughly parallel to highway 178 between Ridgecrest and Trona. The other comes from within the NAWSCL and emerges adjacent to the first noted pipeline just east of the **M**7.1 fault rupture. These pipes are made of multiple pipe materials, including steel, ductile iron, and concrete having diameters of approximately 14 to 16 inches. The welded steel Hilltop Tank is connected to this supply line just east of Ridgecrest.

The SDWC preliminarily reported nine pipe repairs in their system from the **M**6.4 event. There were no reported damages to the supply line coming from within the NAWSCL for that event. Additional repairs were made following the **M**7.1 event. The total number of repairs is unknown at the time of this reporting. Following the **M**7.1 event the supply line coming from within the NAWSCL was damaged and could not be repaired until further notice due to access restrictions.

Figure 28 shows an elephant foots bulge/buckle to the Hilltop Tank, pipe repair, and continued leaking while in service. Figure 27 shows the supply pipeline at the **M**6.4 fault rupture before and after repair. This surface rupture had a zone approximately 400 feet wide at this crossing. The pipeline was damaged and required repair at the edges of this rupture zone (i.e., pipe repairs about 400 feet apart). The western repair was on a steel pipe where a short section of bell (the wide part at end of a pipe section) was cut out. The eastern repair was on a ductile iron pipe where a 17’-4” length of pipe was cut out and replaced.

Following repairs, the supply line was re-pressurized and returned to service before the **M**7.1 event. An additional repair was required within the **M**6.4 fault zone following the **M**7.1 earthquake. This location was not leaking when inspected prior to the **M**7.1 earthquake.

Examination of the repair location by the GEER team indicated a small surface crack within the fault zone in line with the post-**M**7.1 repair.

Figure 30 shows fault offset to concrete segmented pipe crossing the **M**7.1 surface rupture. The pipe was displaced approximately 0.6 m lateral to its axis. On the east end of this movement a slip joint moved on the order of 0.3 m along the pipe axis. One of the 18-foot long segments broke and displaced at about 82-inches west of the joint that slipped. The extending broken piece of pipe displaced somewhat less than 12-inches along the pipeline axis. Three joints west of the broken segment displaced between 1 to 2 inches in axial movement. The pipeline is located at a complicated fault step-over to the west (when looking NW along the fault strike). The main rupture displacing the pipeline in Figure 30 is in line with the surface rupture deforming Highway 178 in compression and right lateral offset. This main rupture dies out just north of the pipeline and starts picking up further west. The fence along the NAWSCL, which is only a few meters north and roughly parallel to the pipeline, was offset by about 4-feet, but further west of the pipeline and roadway offsets. The width of this fault zone is approximately 43 m measured along the fence line.

Following the **M**7.1 event, the SDWC issued a boil water notice and lost water supply once tanks drained their capacity. This required the distribution of bottled water for use due to length of repairs to supply line. Water supply was restored on July 11, 2019 but the boil water notice was not lifted at that time.

Figure 28. Hilltop Tank elephant foot buckle, pipe repair and continued leaking (35.6260, -117.5916).

(a) (b)

(c) (d)

Figure 29. Pipeline damage at **M**6.4 surface rupture crossing. (a) broken pipeline at west side of rupture zone photographed before repair on 7/4/2019 (B. Brooks, USGS). (b) repaired pipeline at west side of fault zone. (c) repaired pipeline at east side of fault zone. (d) leak within fault zone after **M**7.1 earthquake. (35.6443, -117.5369)

Figure 30. Offset of buried concrete segmented pipeline crossing the **M**7.1 surface fault rupture. (35.6492, -117.4822).

Wastewater Systems

Wastewater Systems in Ridgecrest are provided by the City of Ridgecrest Wastewater Division. In Trona they are provided by the County of San Bernardino. In Trona, sewer pipelines were observed to exist in areas experiencing liquefaction and permanent ground movements. There were eyewitness reports of sewer pipeline repairs being made by San Bernardino County the week following the events.

Communications

Little information has been obtained on performance of communications systems, however, there were no anecdotal descriptions of inability to make calls on land or cell lines.

Natural Gas

The Pacific Gas and Electric Company (PG&E) provides natural gas services to approximately 12,543 customers in Ridgecrest and 842 in the Trona area, including some large industrial customers. They do not provide electric power services in the region, which instead is supplied by Southern California Edison Company.

PG&E started assessing potential earthquake impacts as notifications of the July 4, **M**6.4 event were alerted throughout the company and informed by their internal Dynamic Automated Seismic Hazard (DASH) system, the U.S. Geological Survey, news reports, and reports from local employees. Crews were mobilized to evaluate facilities and the gas system, and the

Geosciences Department mobilized a team to evaluate earthquake effects which arrived the morning of July 5. Some primary findings from the initial assessments included surface fault rupture crossing one of the gas transmission line alignments, and non-structural limited damages to the Ridgecrest Customer/Service Center. Leak surveys were performed along gas pipelines including the high resolution Picarro leak detection technology. Pressure and leak testing confirmed that the **M**6.4 fault rupture did not result in a leak of the gas transmission pipe, and assessment of repairs were begun.

The Geosciences and local gas patrol teams were in Ridgecrest at the time of the July 5, **M**7.1 earthquake, and assessment of additional potential damage was initiated. Within a couple hours of the **M**7.1 earthquake, the Geosciences Department reconnaissance team confirmed that the fault rupture crossing the gas transmission line from the **M**6.4 event did not experience additional significant displacement, but that a new fault rupture from the **M**7.1 event occurred several miles to the east, crossing another line in the gas transmission system. As with the prior **M**6.4, pressure and leak testing confirmed that the **M**7.1 fault rupture did not result in a leak of the gas transmission pipe. The pipeline was subsequently excavated and shown to have been deformed as shown in Figure 31 (the deformed section was later replaced). The deformed section of pipe was originally installed in 1955 and is composed of 10.75 inch (outside diameter), 0.188-inch wall-thickness steel pipe (ERW long seam) of grade 42ksi.

Figure 31. Deformed section of 10.75 inch steel gas pipeline following excavation at crossing of M7.1 fault rupture. The surface rupture width in this area was approximately 0.5 m. Photo from PG&E.

Based on initial reports, PG&E mobilized a restoration effort that included staging a local Gas Emergency Operations Center in the Ridgecrest Customer/Service Center yard. During the **M**7.1 event, the Customer/Service Center building experienced additional non-structural damage due

to architectural damage (fallen ceiling tiles) which was repaired the following day to allow the restoration efforts to stage out of the building itself.

Continued reconnaissance during daylight on July 6 included further documentation of the fault characteristics at both pipeline (**M**6.4 and **M**7.1) fault crossings to inform pipeline stress modeling and evaluation of pipeline repair needs. Evaluation of the transmission line integrity indicated that deformation from the **M**6.4 and **M**7.1 surface ruptures did not exceed strain limits for either line, which was confirmed by excavation and inspection. Pipeline reconnaissance and leak inspections were extended throughout the epicentral area as part of due diligence activities to confirm that surface fault rupture or ground failure had not caused significant damage to the gas system. Crossing of gas distribution line and various mapped fault traces at 72 locations in Ridgecrest were visually inspected to confirm no damage.

In addition to new fault rupture, the greater extent and severity of shaking from the **M**7.1 event caused additional or exacerbated general cracking and ground settlement, and leak patrols were continued and extended to identify any damages requiring repair. Some areas of ground settlement apparently related to amplified ground shaking and/or deep liquefaction and lateral spread were observed in the Argus and Trona areas and caused the pavement along Argus Ave. to crack. A PG&E Gas distribution main buried under Argus Ave. was excavated to confirm no damage. Repairs and further detailed assessments of damages and ground failure locations was initiated and are still in progress.

The PG&E Geosciences team collaborated with other agency and research activities, including field mapping, aerial surveys, and seismological evaluation. PG&E Aviation Services and Survey groups acquired high resolution lidar along wide swaths of the fault rupture in vicinity of gas transmission lines, and areas of ground failure in Trona. The post-earthquake lidar is currently being compared against pre-event lidar surveys (including surveys performed on July 1 just before the earthquakes) including change detection processing to confirm field observations and due diligence documentation of the extent of ground failure.

Liquid Fuels

There appears to have been limited effects on liquid fuel systems. Fuels for general public consumption are transported by trucks to fueling stations. Except for possible outage due to temporary electric power service disruption, the fueling stations were observed to remain in service and to be meeting demands. Following the **M** 7.1, a line formed for gasoline at one service station that remained open despite the power outages, when no others were found open.

Electric Power

The Southern California Edison Company provides electric Power Services to the region. Following the **M**6.4 event, there were about 6,900 outages affecting tens of thousands of people reported by SCE (Mosalam 2019).

Financial/Banking

Several automatic teller machines (ATM's) were down during power outages in Ridgecrest.

Los Angeles Department of Water and Power

The Los Angeles Department of Water and Power (LADWP) owns and operates major water and power infrastructure systems in the region. These include the First and Second Los Angeles Aqueducts, hydropower, solar power and wind generation, electric power converter station, and transmission lines. Following the earthquake these facilities were inspected and no damages were reported.

On Twitter (@LADWP), the LADWP reported within the City of Los Angeles one main break and power outages in the Garment district, a portion of San Pedro, and in Granada Hills as potential impacts of the **M**6.4 event. The also reported power outage affecting about 100 customers in the Encino/Valley Glenn area resulting as a potential result of the **M**7.1 event.

Dams and Reservoirs

The closest dams and reservoirs are at North and South Haiwee, approximately 53 km north of the epicenters. The LADWP reported no indication of movement or damage of any kind after undertaking inspections and surveys.

The United States Army Corps of Engineers (USACE) owns and operates Lake Isabella Dams in the town of Lake Isabella, located more than 50 miles from the epicenters. The USACE reported no signs of distress after a series of inspections following both events (Press report).

Fire Following Earthquake

Following the **M**6.4 event, Dr. Charles Scawthorn of SPA Risk, LLC, contacted the Kern County Emergency Operations Center and Fire Department Incident Commander who indicated there was one structural fire, cause still under investigation and not yet confirmed as earthquake-caused (as of July 5 morning) (described further in Section 2.5). There were also numerous reports of gas leaks, each of which requires a structural fire response (but is not a fire). Following the **M**7.1 event, within 200 minutes after the event there were 14 fire-related responses in Kern County, 7 of which were structure fires. Six of these were in Ridgecrest and eight were in Bakersfield and Shafter 80 miles or further from the epicenter. This information was provided courtesy of C. Scawthorn (oral communication, July 5, 2019).

2.3 Liquefaction and Related Ground Failure

Conditions for susceptibility of sediments to liquefaction are not abundant in Indian Wells Valley due to the lack of surface water and deep groundwater table. Searles Valley, located to the east of Indian Wells Valley, contains the dry Searles Lake, which is currently utilized for mineral mining operations by the Searles Valley Mining Company. Searles Lake consists of

Quaternary lacustrine deposits that are highly calcareous sand, silt, or clay at locations that were a kilometer or more from shore at the time of deposition, and well-sorted sands and gravels nearer to the shore (Smith 2009). Surficial sediments around the perimeter of the lake are generally Holocene sands and gravels. Surface water was visible in portions of Searles Lake, and shallow groundwater was observed at several locations around the perimeter of the lake. As a result of the shallow groundwater and sandy soil conditions, liquefaction and lateral spreading was observed near multiple locations along the lake perimeter. The GEER team visited Trona and Argus, towns situated near the northwestern margin of Searles Lake, to document liquefaction effects in the region. Figure 32 shows the locations of these towns with respect to the limits of Searles Lake.

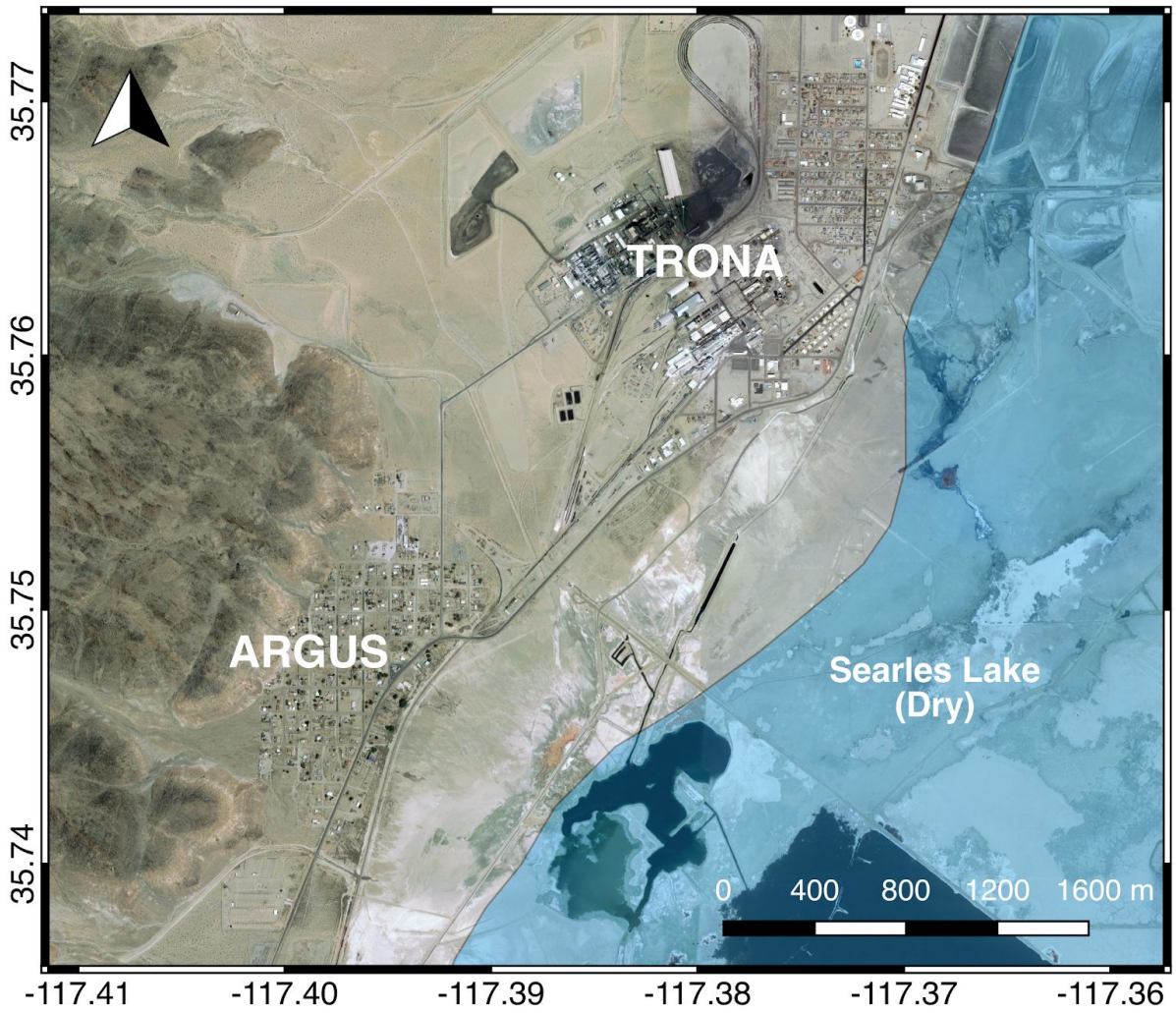

Figure 32. Map of Argus and Trona showing showing margin of Searles Lake.

Figure 33 highlights the region of Trona investigated by the GEER team. Liquefaction features were apparent throughout this region. Yellow markers indicate regions where the team

photographed sand boils (e.g., Figure 34). The team did not perform an exhaustive survey of all sand boils in Trona, and it is therefore possible that sand boils existed in additional areas. Sand boils were encountered along the southern margin of Trona near the northern margin of Searles Lake. The GEER team could not access Searles Lake near Trona because it was protected by a chain link fence with barbed wire at the top. Ground cracks caused by extensional strain due to lateral spreading were apparent near the sand boils, and throughout the region investigated by the GEER team. The orientation of the extensional cracks was highly variable. Many cracks trended toward the northeast, parallel to the lake perimeter, but many other cracks were at different angles. We interpret this to indicate that the lateral spreading was predominantly toward the lakebed, but spreading occurred in many other directions as well, possibly due to the influence of structures on ground displacements, or due to ground lurch. In addition to the extensional ground cracks (Fig. 35), compressional features were also observed in various regions (Fig. 36), as evidenced by buckled concrete curbs, and regions where the asphalt pavement cracked and rode up over adjacent pavement. Structures appear to have been affected by the lateral spreading, including the restaurant shown in Fig. 37, which experiences wall cracks in the **M**6.4 event that were widened in the **M**7.1 event. It is possible that many cracks pre-dated the earthquake sequence, and were subsequently widened by the earthquake. Considering the complicated deformation patterns and possibility of pre-earthquake cracks, we suggest that future remote sensing surveys may be valuable at this site.

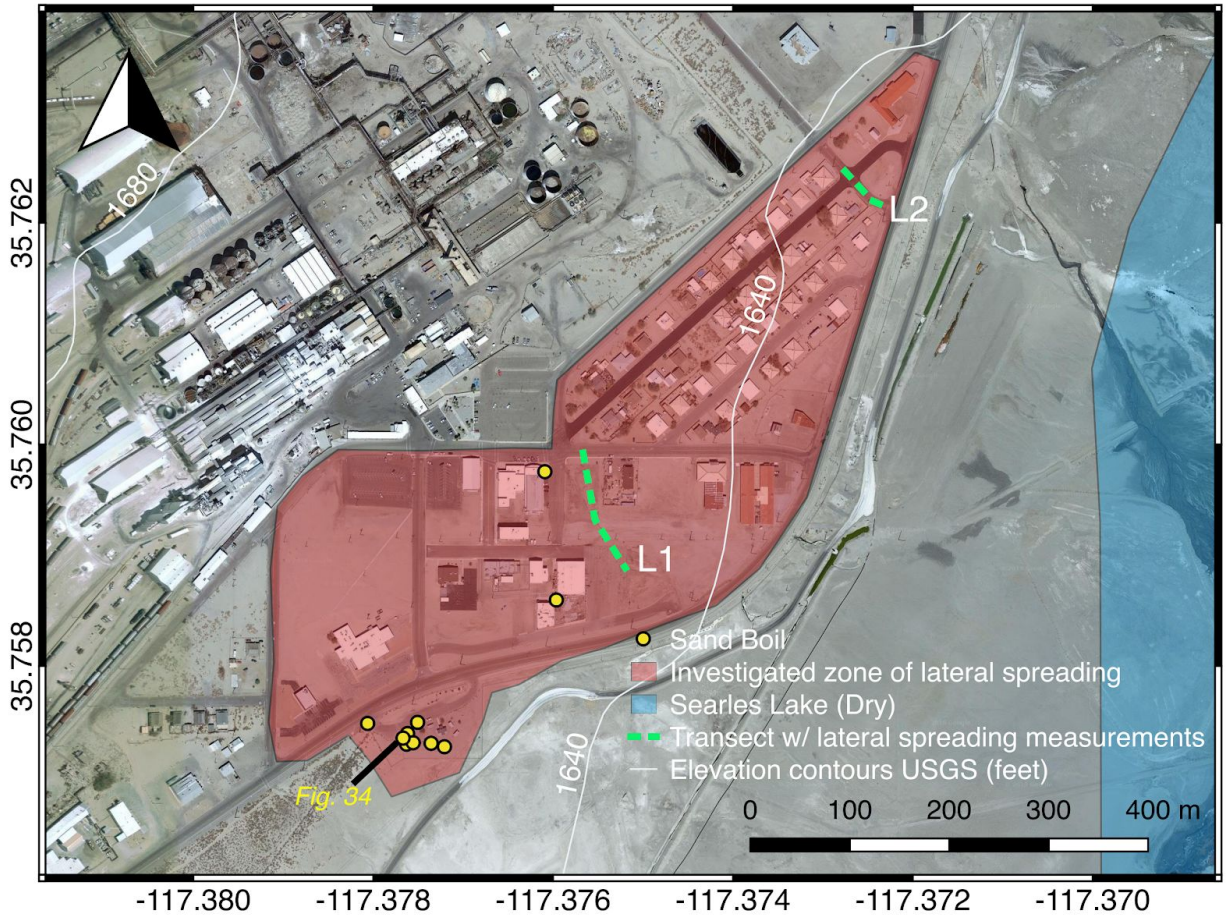

Figure 33. Map of Trona showing region investigated by the GEER team, along with selected sand boils that were photographed by the team. Lateral spreading features, including tensile cracks and compressional features, were observed throughout the investigated zone.

Figure 34. Sand boil near margin of Searles Lake in Trona. Photo by Scott Brandenberg, (35.7573, -117.3776).

Figure 35. Ground cracks due to liquefaction-induced lateral spreading in Trona. Photo by Scott Brandenberg, (35.7626, -117.3731).

Figure 36. Ground compression, including buckled curb, due to liquefaction-induced lateral spreading in Trona. Photo by Scott Brandenberg, (35.7623, -117.3725).

Figure 37. Esparza Restaurant building in Trona that exhibited cracked walls, (A) After the **M**6.4 earthquake and before the **M**7.1 and (B) after the **M**7.1 earthquake. Following the M7.1 earthquake, the horizontal and vertical cracks widened, the roof showed damage and a sand boil appeared at the base of the crack shown in the photo. Photos by Christine Goulet (35.7595, -117.3757).

Figure 38 displays the areas of Argus surveyed by the GEER team. Similarly to Trona, many liquefaction related features were observed throughout Argus. The ground surface in the area shown as experiencing liquefaction has a gentle slope. The ground surface exhibited

extensional cracks ranging from less than a millimeter to approximately 10 cm in width. The lateral spreading features became less frequent with proximity to the hills to the west of Argus. The lateral spreading features were more pervasive along the axis of a large alluvial fan coming from the ridge to the west. A photo survey was performed along a transect on A Street, approximately along the axis of the alluvial fan as shown in Figure 38. The transect was 1,500 feet long, and the elevation difference (from USGS Topographic Map) ranged from 1640 to 1720 MSL (east to west), indicating an average ground surface slope along the transect of approximately 5%. The extensional features were measured along the transect and the cumulative displacement is shown in Figure 39. The sum of ground cracks measured across the 1500-feet long photo survey was approximately 22 inches.

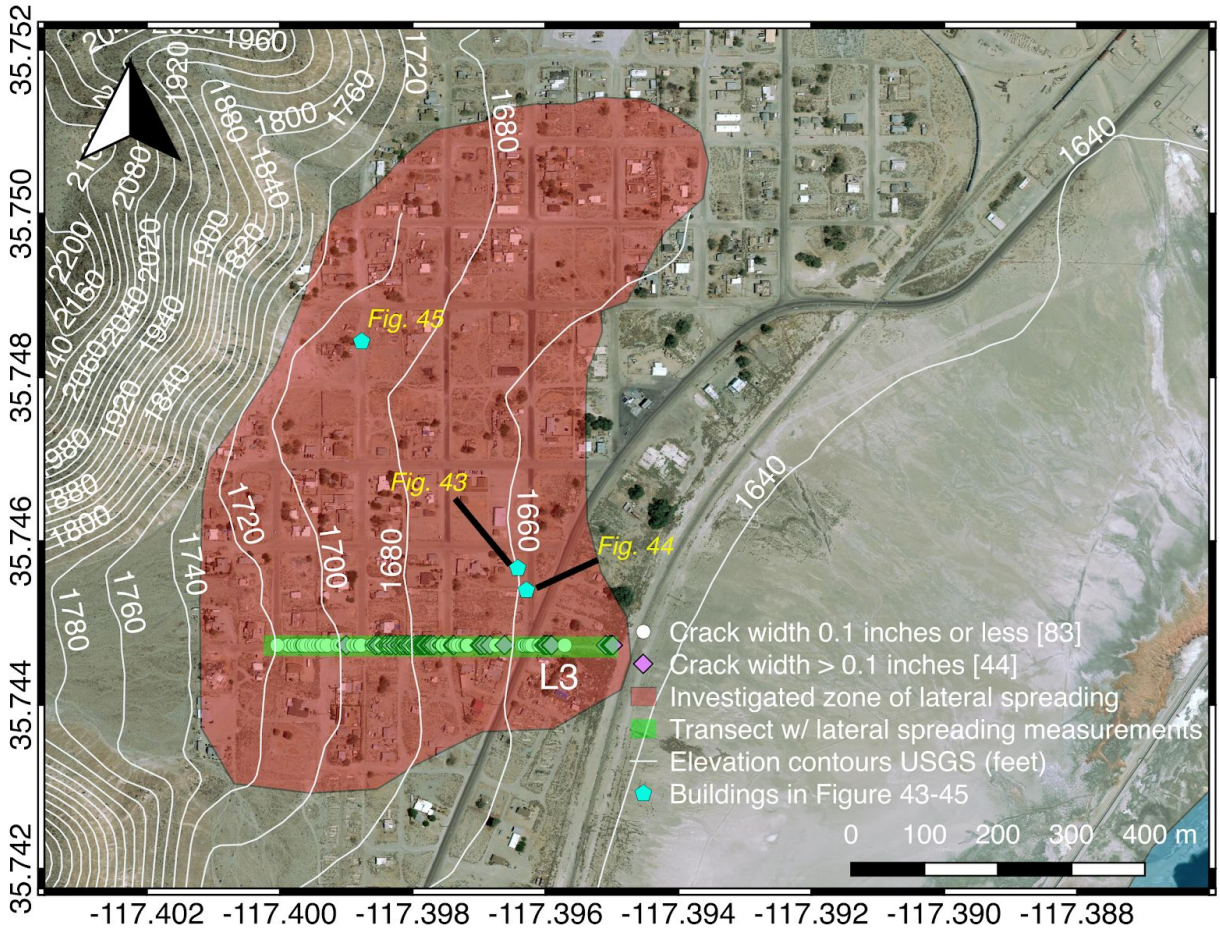

Figure 38. Map of Argus showing region investigated by the GEER team. Lateral spreading features, including tensile cracks and compressional features, were observed throughout the investigated zone. Lateral spread cracks were measured along a transect on A Street.

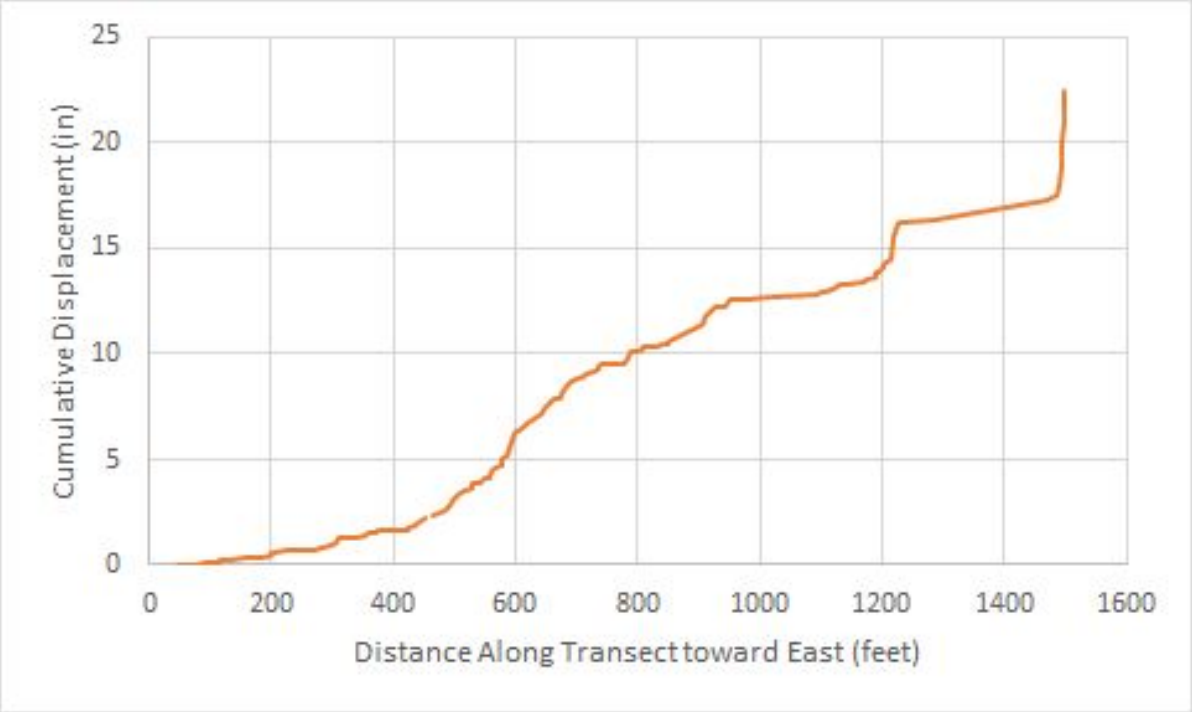

Figure 39. Cumulative distribution of crack width along transect along "A Street" in Argus

On July 11, Scott Brandenberg met with Shawn Barker, who owns a construction company in Argus. Shawn recently installed a well in the hills to the north of Trona as part of a lime mining operation. The well extends to a depth of 110m (360 ft), and is perforated from 91.4m (300 ft) to 109.7m (360 ft) depth with the intention of pulling water out of the rock formation that begins at a depth of 91.4m (300 ft). Mr. Barker indicated that the depth to groundwater in the well was 90.8m (298 ft) before the earthquake, and subsequently rose to 88.7m (291 ft) soon after the **M**7.1 event, and is now at 87.5m (287 ft) and continues to rise. The location of the well is (35.7700, -117.3898), and the altitude is 549m based on a waypoint collected using the GPS Tracks iPhone app. The elevation of the lakebed near south Trona is approximately 500m. Groundwater was encountered near the surface at this location, indicating that the groundwater elevation at the well location is approximately 40m lower than the groundwater elevation at the lakebed. We initially reached out to Mr. Barker after hearing about the increase in water elevation in his well because we thought this could be due to liquefaction. However, we now consider any link with liquefaction at the well site to be unlikely considering that the water table is very deep and in a rock formation.

2.4 Ground Motions

Recorded Ground Motions

The **M**6.4 and **M**7.1 events were recorded by 494 and 738 ground motion recording stations, respectively, which belong to nine different networks (Tables 1 and 2). We have compiled preliminary source, path, and site metadata to provide insights into basic attributes of the mainshock event ground motions.

Table 1. Stations and networks that recorded 7/4/2019 **M**6.4 event (IRIS Event ID 11056847, IRIS 2019a)

Network Code	# of Stations	Network Name
CI	294	Southern California Seismic Network (SCSN), Caltech
NP	65	National Strong-Motion Project (NSMP), USGS
CE	57	California Strong Motion Instrumentation Program (CSMIP), CGS
NC	36	Northern California Seismic Network (NCSN), USGS
BK	18	Berkeley Digital Seismic Network (BDSN), University of California at Berkeley
AZ	17	ANZA Regional Network
WR	4	California Division of Water Resources (CDWR)
NN	2	Nevada Seismic Network, UNR/NSL
PG	1	PG&E
Total	**494**	

Table 2. Stations and networks that recorded 7/5/2019 **M**7.1 event (IRIS Event ID 11058875, IRIS 2019b)

Network Code	# of Stations	Network Name
CI	313	Southern California Seismic Network (SCSN), Caltech
CE	253	California Strong Motion Instrumentation Program (CSMIP), CGS
NP	43	National Strong-Motion Project (NSMP), USGS
BK	20	Berkeley Digital Seismic Network (BDSN), University of California at Berkeley
NC	69	Northern California Seismic Network (NCSN), USGS
PG	10	PG&E
WR	7	California Division of Water Resources (CDWR)
Total	**738**	23 others

In collaboration with the Natural Hazards Risk and Resilience Research center (NHR3), we downloaded volume 1 (digital uncorrected) data from the mainshock (**M** 7.1) and its main foreshock (**M** 6.4) on July 6-7 2019 from the CESMD web site. Additional M7.1 ground motions were downloaded and processed July 30-31 2019. In total, 1232 records were downloaded and processed using standard processing procedures developed in the Pacific Earthquake Engineering Research center for Next-Generation Attenuation (NGA) projects (e.g., Ancheta et al. 2014), which removes any static offset effects that might otherwise be present and filters the ground motions to minimize effects of low-frequency noise.

We have compiled the V_{S30} site parameter for each station (i.e., time-averaged shear wave velocity in upper 30 m of site). For 285 stations, we retrieved V_{S30} values from the NGA-West2 site database (Seyhan et al. 2014). For the remaining stations, which were not considered in the NGA-West2 project, we estimate site parameters using two proxy-based V_{S30} estimation models. The first is a raster map utilizing surface geology and topographic slope (Wills et al. 2015), and uses kriging methods to consider proximity to existing in situ V_S measurements (Thompson 2018). Due to limited seismic velocity measurements in the region, direct use of the Wills et al. (2015) model is similar to the use of the kriging method. The second model is that of Yong (2016), which uses a three-part geomorphometric terrain classification scheme of Iwahashi & Pike (2007). Final V_{S30} values were computed for each site that lacked situ V_{S30} measurements using a weighting scheme of ⅔ and ⅓, respectively, for each of the aforementioned models. These weights were based on previous experience of proxy-based V_{S30} predictive power from past NGA studies (e.g., Seyhan et al. 2014, Ahdi et al. 2017).

Rupture distances (R_{RUP}) and distances to the surface projection of the fault (R_{JB}) are identical for the preliminary finite fault models, because these models reach the surface and have vertical dips (90 degrees). These distances have been evaluated using the simplified linear representation of slightly irregular (variable strike) surfaces provided by E. Thompson (personal communication, 2019) and are shown in Figure 1. The sources are taken as strike-slip with magnitudes of 6.4 and 7.1.

Figure 40 compares median-component (RotD50, as given by Boore 2010) ground motions as a function of rupture distance for three general groups of site class (> 760, 360-760, and < 360 m/s), using the intensity measures of peak acceleration (PGA) and pseudo-spectral acceleration response spectra (PSA) for two oscillator periods (0.2 and 1.0 s). Also shown in Figure 40 is the average prediction of four NGA-West2 models (Abrahamson et al. 2014; Boore et al. 2014; Campbell and Bozorgnia 2014; Chiou and Youngs 2014) along with a range of plus and minus one total standard deviation. The ground motion models are plotted for V_{S30} = 360 m/s. Three key findings of this preliminary analyses are:

1. The ground motion models do not appear to have appreciable bias relative to the data for the intensity measures considered (formal residuals analyses are pending);

2. The California-specific path model used in the models captures relatively well the attenuation of ground motions with distance;
3. Ground motions are amplified as site condition softens, with the largest amplification at the longest periods. This is consistent with typical patterns of behavior in California.

Figure 41 shows 5% damped PSA for six stations most proximate to the **M**7.1 mainshock rupture (CCC, CLC, TOW2, 5419, SRT, Q0072), which are shown in Figure 1. The left panel of Figure 41 shows that the RotD50 component of these records is reasonably consistent with predicted spectra from ground motion models. The right panel shows that the motions are generally at or below the risk-targeted maximum considered earthquake (MCE_R) levels, with the exception of CLC, which exceeds MCE_R for periods below about 0.5 sec. Along with CLC, other near-fault motions (CCC and TOW2) exceed design levels. The corrected ground motions have been rotated into fault-normal (FN) and fault-parallel (FP) components. Station CCC is located south of the fault, aligned with the fault strike, and hence would be expected to experience forward directivity effects. The FN component carries most of the energy, producing the maximum component at long periods (> 1 sec). The FN component also controls the maximum component for TOW2. Station CLC is located near the epicenter, and hence is in a backward directivity region. This record has appreciably lower long-period spectral ordinates than CCC and does not have polarization of the energy in the FN direction.

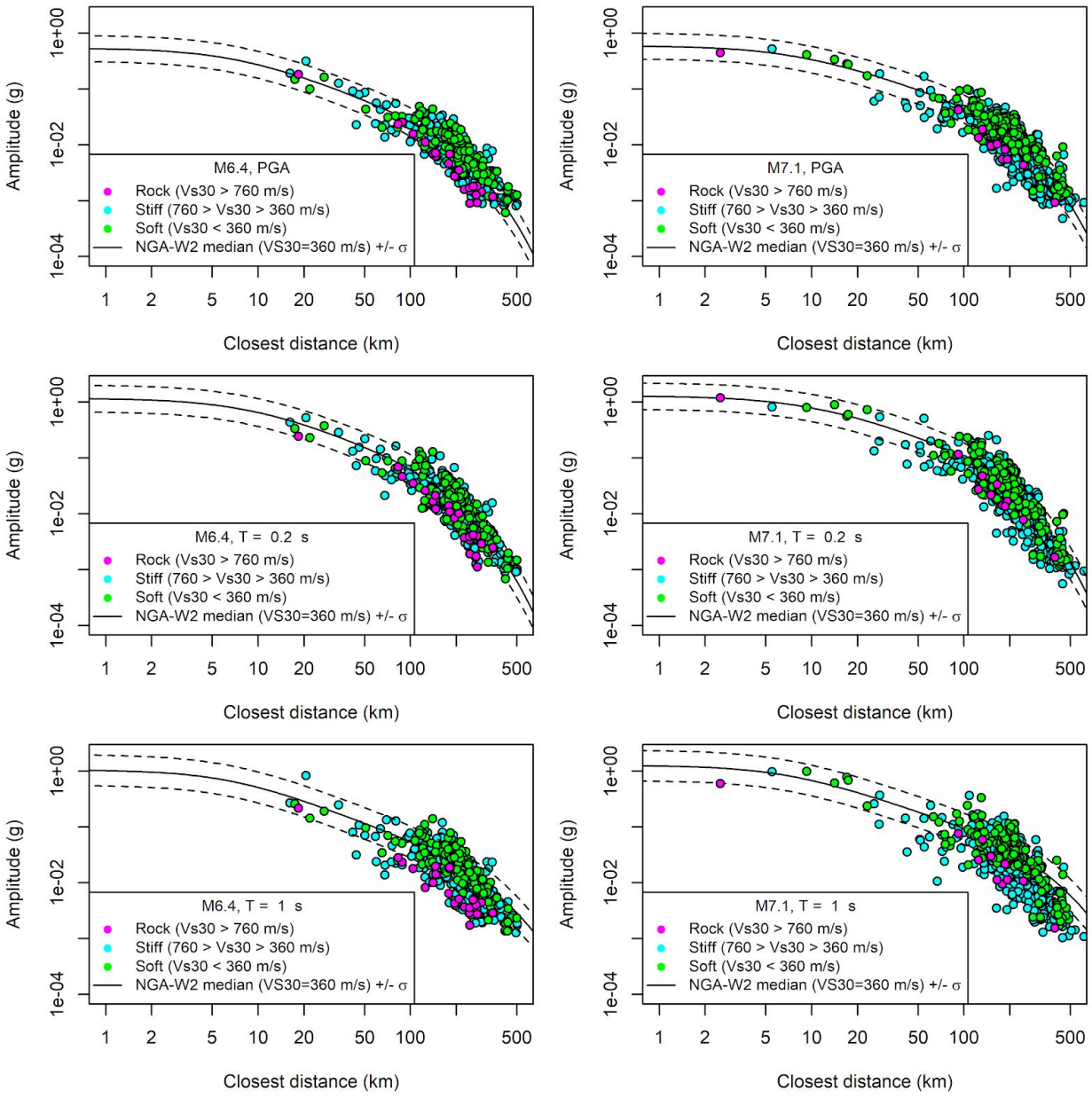

Figure 40. Attenuation with distance of ground motions from **M**6.4 event (left column) and **M**7.1 event (right column). RotD50 component PGA and PSA at 0.2 and 1.0 sec.

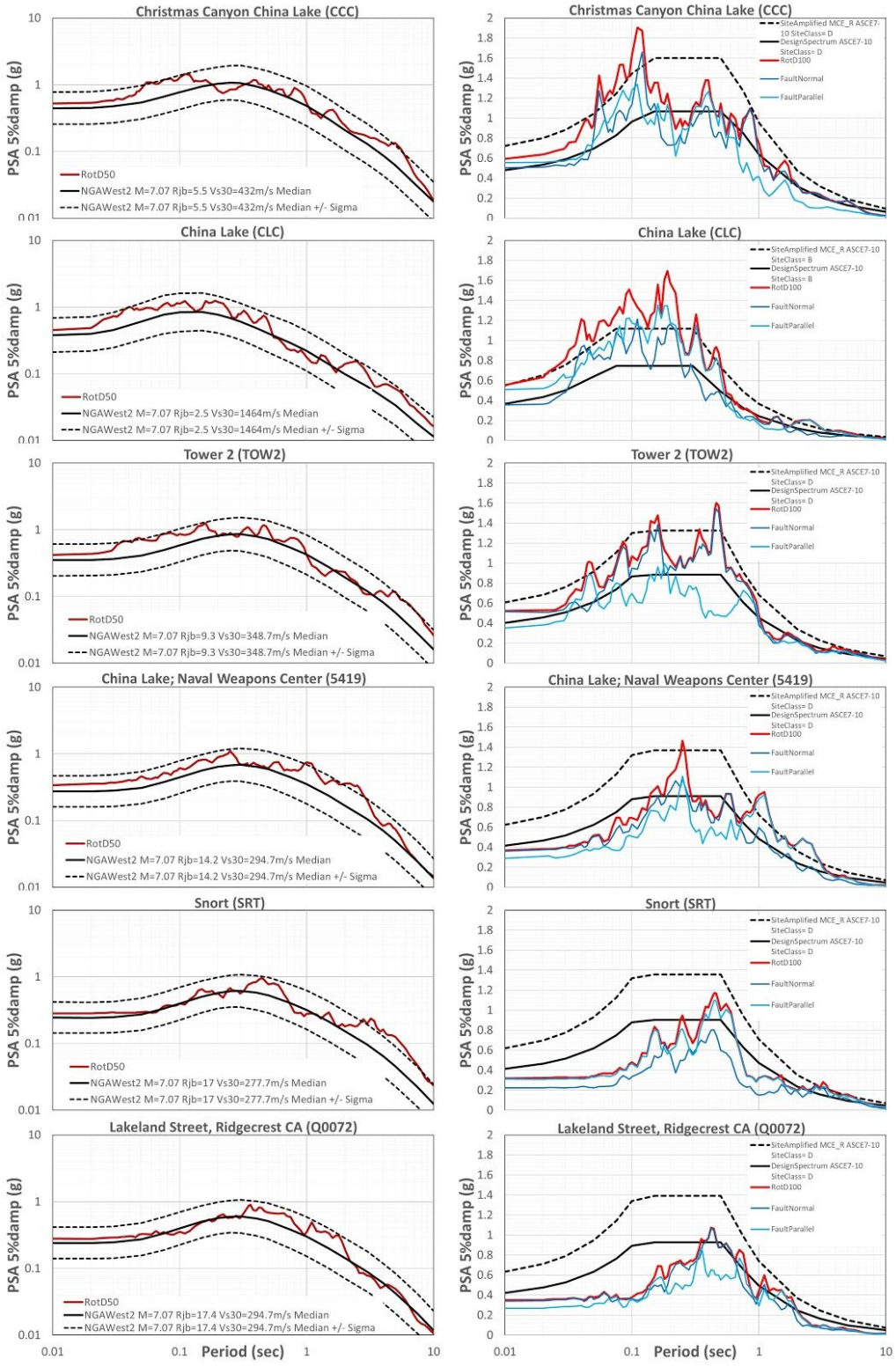

Figure 41. Pseudo-acceleration spectra for stations proximate to fault rupture of **M**7.1 event. Right plots show RotD50 components (data) and median predictions from NGA-West2 models. Left plots show RotD100, fault-normal, and fault-parallel components, along with design and MCE_R spectra (ASCE 7/10).

Temporary Arrays

Between approximately July 6-11 2019, scientists from USGS, UC Riverside, and the Scripps Institution of Oceanography (UC San Diego) have deployed 23 temporary seismic instruments, several of which were coordinated with the GEER team. The locations of these instruments are shown in Figure 42. Instruments are installed mainly along the **M**7.1 fault, but also in developed areas (Ridgecrest and Trona). The array in Trona spans from shallow stiff soil to soft liquefiable soils. Analysis of data recovered from these arrays has not yet occurred.

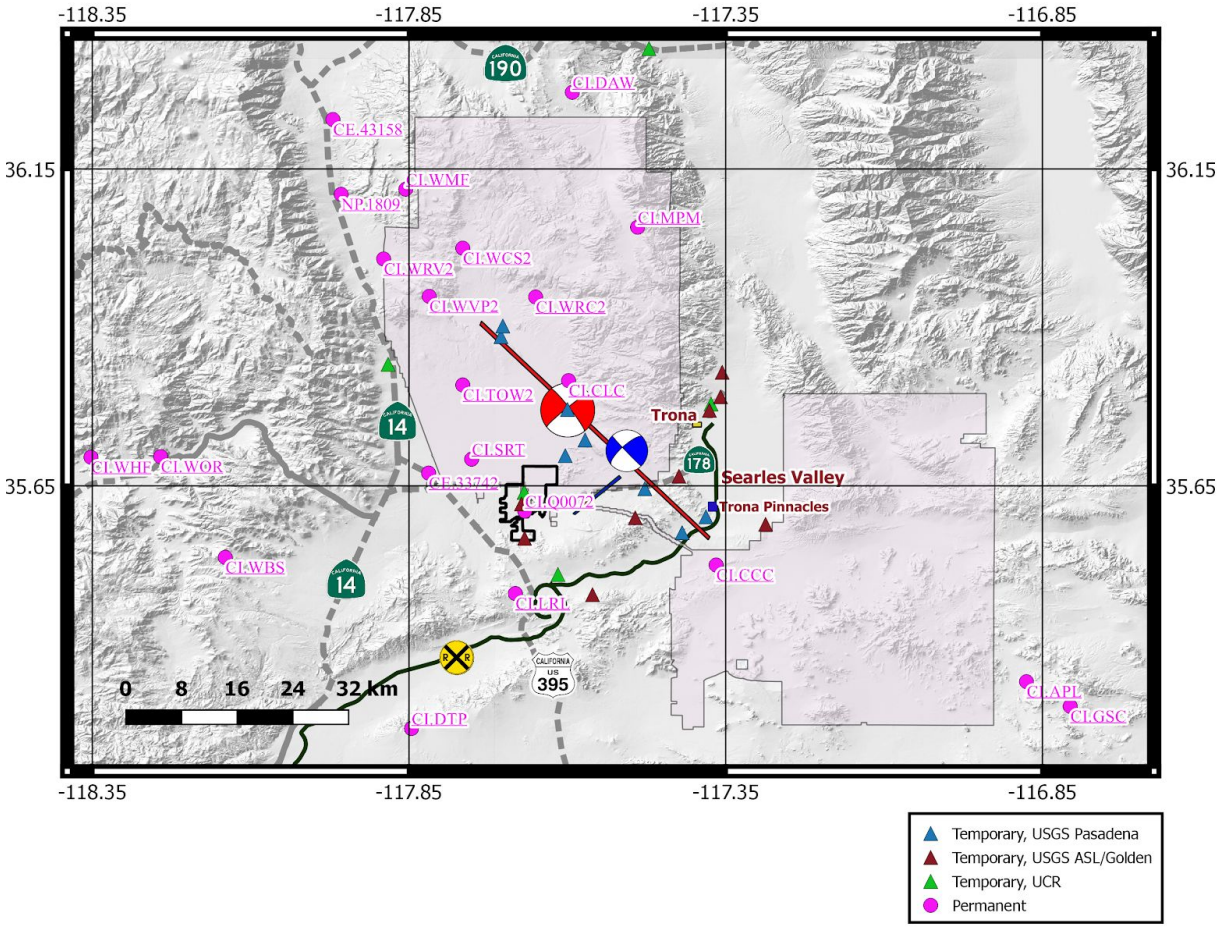

Figure 42. Locations of temporary arrays to record aftershock ground motions, with permanent stations also shown for reference. Location data courtesy of J. Steidl and E. Cochran (pers. communication, 2019).

Fragile Geologic Features

Fragile geologic features (FGFs, which include precariously balanced rocks, PBRs) can be used to constrain the maximum level of ground motion that has occurred at a site (Brune 1996). A good candidate site for study of FGFs is the Trona Pinnacles, designated as part of the California Desert National Conservation Lands (https://www.calwild.org/trona-pinnacles/; location shown in Figure 42). The Pinnacles comprise over 500 tufa (geothermally-created formations from calcium carbonate precipitation) spires. The spires vary in shape and size and have well-documented pre-event geometries. The tufa spires are brittle formations and some of them are segmented from aging and earthquake events. The spires are susceptible to damage from faulting, but are especially susceptible to toppling from ground shaking, hence can be used to estimate ground shaking at a site. A SCEC-GEER based team visited the Trona Pinnacles on July 12 and found several damaged spires. The Jet Propulsion Laboratory (JPL) Unoccupied Aerial Vehicle (UAV) team was dispatched on the site on July 14 to perform the 3D reconstruction of one damaged spire. The University of Washington (UW) UAV team has performed the same operation on additional spires. A multi-agency proposal coordinated by SCEC is being submitted to NSF to complete lidar surveys over the Pinnacles as well.

2.5 Structural Performance

Structural Performance on Liquefied versus Non-liquefied Soils

The location of more heavily-damaged structures in Argus appeared to coincide to some degree with areas with greater evidence of lateral spreading. Part of this is due to the lateral displacements, but it appears that there was a difference in the characteristic of shaking in areas exhibiting greater liquefaction effects. There is likely a greater depth of recent alluvium near the central axis of the alluvial fan and corresponding lower shear wave velocity that would be encountered in such deposits, and these deposits also were subject to liquefaction (see Section 2.3).

Figure 38 shows the locations of several buildings that illustrate these effects and described here. Figure 43 shows a heavily damaged structure (Structure A1) which is on the alluvial fan, near many liquefaction-induced lateral spreading cracks (as shown in Figure 44). In contrast, Figure 45 shows an unreinforced stone structure with a stone chimney (Structure A2), which is within a few blocks of the house shown in Figure 43, but has relatively little damage. Structure A2 is near the base of the mountain, with no observable effects of liquefaction on the ground in the immediate vicinity.

Figure 43. Example of more heavily damaged Structure A1 in vicinity of liquefaction – induced ground cracking (upon alluvial fan deposits – see canyon visible behind structure). (35.7457, -117.3964)

Figure 44. Example of liquefaction-induced lateral spreading ground cracking in vicinity of Structure A1 (at right of photograph). (35.7454, -117.3963)

Figure 45. Example of less-heavily damaged Structure A2, not in vicinity of liquefaction – induced ground effects (at base of mountain). (35.7484, -117.3988)

NAWSCL Structures

Structures within the NAWSCL experienced significant damage that affected facility mission readiness and caused many of the Navy staff to relocate temporarily to other locations. An assessment phase was undertaken in the first 2-3 weeks following the event to identify the damaged structures requiring repairs. As of this writing, the majority of the workforce has returned to the base, which will accelerate the process of performing detailed assessments of facilities and technical infrastructure. Further details on damage in the base cannot be disclosed due to Navy policy related to operational security considerations.

Wood-frame Structures

The main form of construction in Ridgecrest is single-story wood-frame structures; these structures are mainly constructed with stucco walls and have slab-on-grade foundation (personal communication, Keith Porter, 2019). Engineering experience indicates that this form of construction performs well during seismic excitations. Field reports after the **M**6.4 and **M**7.1 events, anecdotal reports from Ridgecrest residents, and observations made by the reconnaissance team from the outside of many such structures support the past experience. There was a report of a single fire break out after the **M**6.4 event, which was suggested to be due to a gas leak from gas pipe rupture (Figure 46).

There have been multiple reports of damage to the interior of wood-frame dwellings without any visible damage from the street. This type of damage was reported during a few of the CA Clearinghouse Briefings and anecdotal reports from Ridgecrest residents.

Figure 46. Damaged wood-frame house due to gas leak fire in Ridgecrest (35.6202, -117.6612) Photo credit: Farzin Zareian

Mobile homes

Mobile homes suffered significant damage after the **M**6.4 and **M**7.1 events. The reconnaissance team observed a broad spectrum of mobile home damages during their visit to the Ridgecrest mobile home park after the **M**6.4 and **M**7.1 (Figures 47 and 48). The **M**6.4 event caused two mobile home collapses (Figures 47a and 47b), one tilted (Figure 47c); and many with foundational support movement or interior and exterior damages (Figures 47d, 47e, 47f). Locals observed one of the mobile homes lifted off and dropped on the ground during the **M**6.4 event leading to its supports punching through its floor Figure 47b. Both mobile homes that collapsed during the **M**6.4 event have been in place for more than ten years. Movement of supports did occur on mobile homes that moved to the park recently, but these did not collapse.

Figure 47. Damaged mobile homes in Ridgecrest after M6.4 event (35.6444, -117.6733) Photo credit: Farzin Zareian

The **M**7.1 event caused collapse in many mobile homes most of which underwent support movement during the **M**6.4 (Figure 48). This observation leads to the conjecture that during the life of a mobile home and experiencing multiple moderate seismic excitation, damage to the structural components – mainly in the supports – accumulate and eventually leads to significant

tilting and collapse. The two collapsed mobile homes during the **M**6.4 event had been in place for more than a decade; the mobile homes collapsed during the **M**7.1 event had mainly suffered support damage due to the **M**6.4 event.

Figure 48. Collapsed mobile homes in Ridgecrest after M7.1 event (35.6444, -117.6733) Photo credit: Jawad Fayaz

Hospital

Ridgecrest Regional Hospital after the **M**6.4 and **M**7.1 events did not suffer any observable structural damage; much of the damage was limited to nonstructural components. These damages, however, triggered the shutdown of the hospital after the **M**6.4 event. The reconnaissance team visited the hospital after each event.

Three independent sets of nonstructural damages were observed after the **M**6.4 event. The first one is related to the breakage of copper pipes on three out of four water pumps in the mechanical housing (at the penthouse level, see Figure 49a). This breakage led to release of hot and cold water into the elevator shaft. In the second set of nonstructural damage, a hot water pipe leaked in the ceiling of one of the operation rooms (i.e., OR1) which led to release of water on the operation room's floor (See Figure 49b). Lastly, partition walls were cracked, and some sprinklers were displaced with damage (Figures 49c, 49d, 49e, 49f). Partitional wall cracks were mainly vertical and horizontal; some diagonal shear crack were observed around openings.

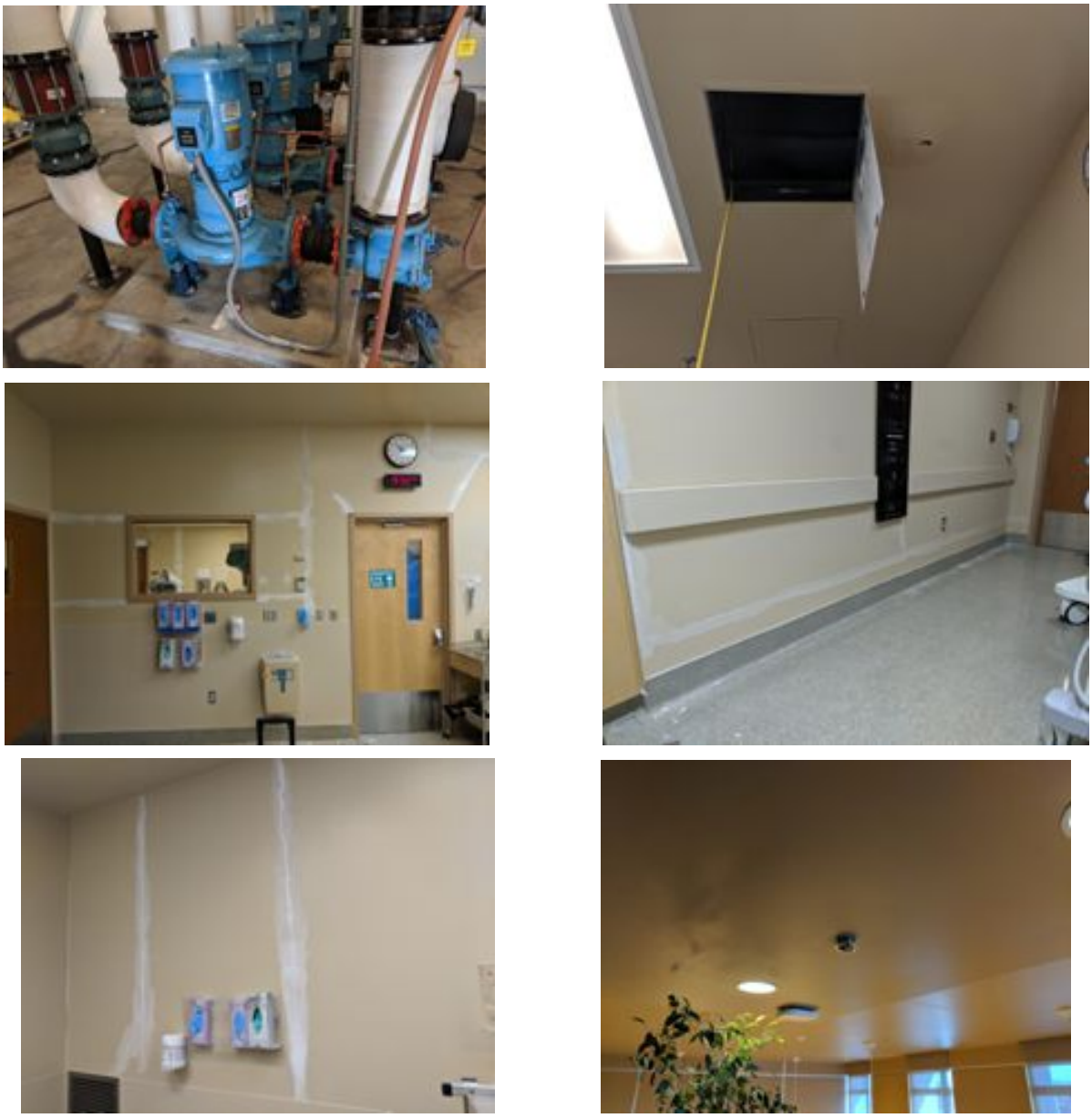

Figure 49. Damages to Ridgecrest Regional Hospital after the **M**6.4 event (35.6410, -117.6707) Photo credit: Farzin Zareian

The reconnaissance team observed similar damages during its visit to Ridgecrest Hospital after the **M**7.1 event. The main additions to the damage were one pipe leakage in one of the patient rooms (Figures 50a and 50b), movement of ceiling tiles (Figure 50c), and movement of office equipment and supplies (Figure 50d). There has been no observed structural damage.

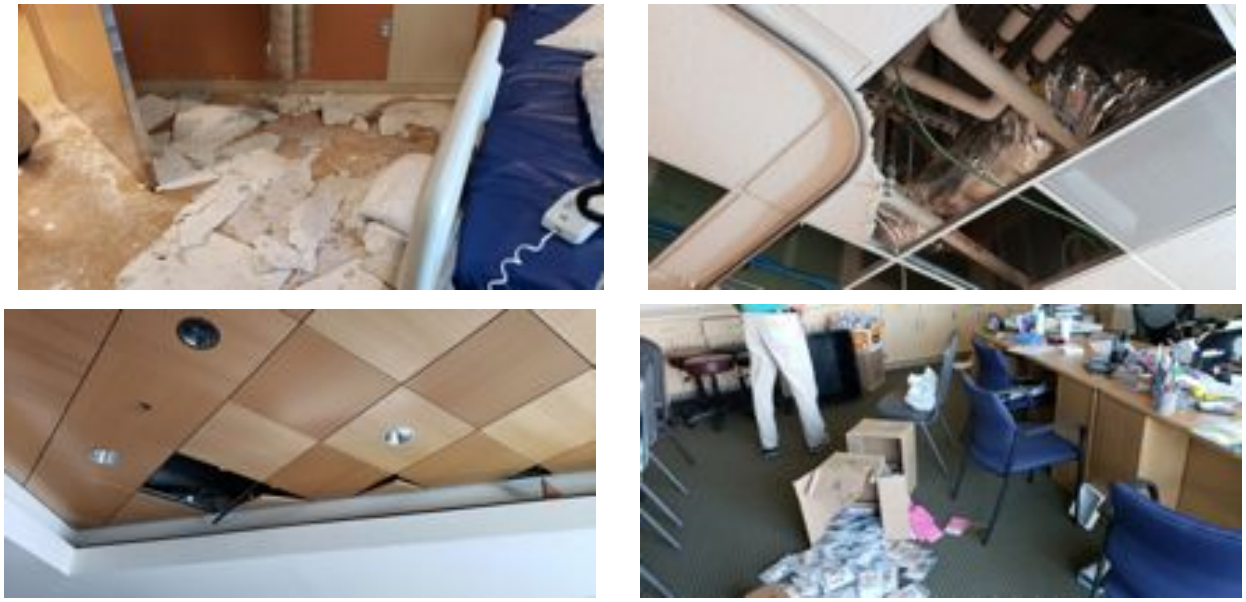

Figure 50. Damages to Ridgecrest Regional Hospital after the M7.1 event (35.6410, -117.6707) Photo credit: Jawad Fayaz

Damage masonry components

Horizontal and vertical cracks were induced and widened in masonry walls during the **M**6.4 and **M**7.1 events in Trona (See Figure 48a). These damages were related to possible liquefaction-induced lateral spreading, which also caused damages to pavements (See Figure 51c). Yard walls were displaced in Trona and Ridgecrest resulting in fall over of walls (see Figure 51d). There have been reports of chimney failure in Trona after the **M**7.1 event (Figure 51b).

Figure 51. Damages to Masonry components after the M7.1 event (a: 35.7595, -117.7357, b: 35.7592, -117.3766, c: 35.7595, -117.7357, d: 35.6444, -117.6720) Photo credit: Christine Goulet and Jawad Fayaz

Ridgecrest Cinema

After the **M**7.1 event, The roof of one theatre (of a total of eight theaters) in Ridgecrest Cinemas collapsed; this led to the closure of the cinema (communication via EERI's CA Clearinghouse Briefing #4). According to this reference (i.e., Fred Turner), the cause of this collapse has been the separation of wood roof trusses from concrete masonry walls (Figure 52).

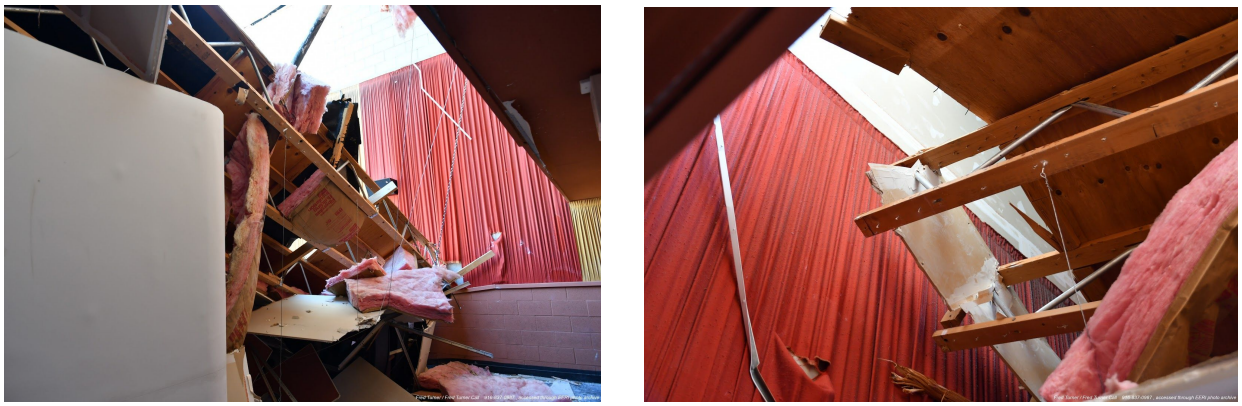

Figure 52. Observation of collapsed roof in Ridgecrest Cinema after **M**7.1 event (35.6499, --117.6715) Photo credit: Fred Turner

Bridges

The reconnaissance team visited the Ridgecrest – US-395/Brown Road Bridge after each of the **M**6.4 and **M**7.1 events. This bridge is instrumented through the California Strong Motion Instrumentation Program (CSMIP) (Station #3372). The bridge has a box-girder deck with seat-type and skewed abutment. During both visits, no damage was observed on the column and deck of the bridge (Figure 53).

Figure 53. Observation of Ridgecrest – US-395/Brown Road Bridge after M7.1 event (35.6696, -117.8187) Photo credit: Jawad Fayaz

3.0 Imaging

3.1 Digital Elevation Models (DEMs) from Photographs

Photographic imaging has been performed for the purpose of developing DEMs of ground failure features. Ground- and helicopter-based imagery was performed in the NAWSCL and Unmanned Aerial Vehicle (UAV) imagery has been used outside of the base.

USGS and CGS collected many thousands of high-resolution (DSLR) photos from the ground and air within the Navy base. In many cases, stereo overlap and geo-tags were intentionally collected so as to allow for SfM methods and that processing is underway. The entire length of the maximum slip zone was photographed with stereo overlap during very low altitude (approx. 60 m above ground) as well as from the ground at a distance of about 10 m away on either side. At sites of interest for recovering a fault slip displacement vector, the feature of interest was encircled while taking photos pointed inward at the offset feature. As much as possible, the zoom setting was maintained as a constant during these efforts to carefully document the fault rupture.

UAV imagery outside of the NAWSCL has been completed at the locations shown in Figure 54 by GEER and collaborating organizations (UNR/ASU, JPL, UCLA, and UW Rapid). These deployments had different objectives regarding level of precision and extent of coverage.

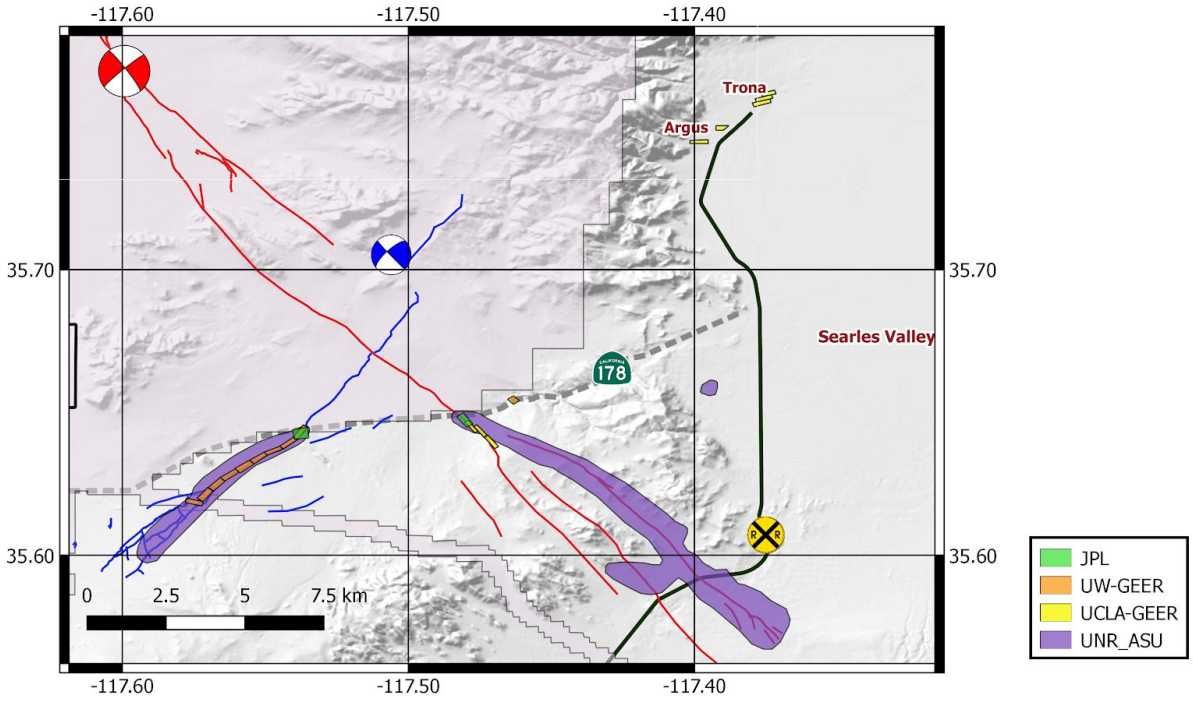

Figure 54. Map of regions imaged by GEER team and collaborators outside of the NAWSCL using UAVs.

Between July 5-8, the UNR/ASU team collected UAV images along the entire publicly accessible areas of the main strands of both the **M**6.4 and **M**7.1 ruptures south of Highway 178. Low resolution models for the southern part of the **M**7.1 rupture have been produced and high resolution models are in process. Due to field issues with the Trimble R10 in the field, ground control points were not collected. It is anticipated that ground control points from the other GEER activities can be incorporated into the models for geo-referencing. The UNR/ASU anticipates producing detailed maps of the ground deformation once high resolution models are completed, and may reimage to evaluate scarp degradation.

On July 9, 11, and 15, the Jet Propulsion Laboratory (JPL) team collected UAV images of the **M**6.4 and **M**7.1 surface ruptures that had previously been mapped by the GEER team in the field. These regions extended from where the surface ruptures crossed Highway 178 to approximately 500m toward the southwest (**M**6.4) and southeast (**M**7.1). Ground control points were surveyed and included in the images for the purpose of geo-referencing. The JPL team plans to re-image the same region at various future times for the purpose of quantifying after-slip. Figures 55-56 show samples of the initial imagery results from the UAV surveys completed by the JPL team at the locations of detailed mapping of the **M**7.1 and M6.4 ruptures, respectively. They produced 2 cm posting digital surface models and orthomosaics of the two locations. Average ground sample distance is 1.5 cm and the products are orthorectified using ground control points that were surveyed using RTK GPS. They plan to return to assess postseismic deformation.

One product of the JPL team is before-after video imagery of fault rupture. One such file for the **M**7.1 rupture is attached to the pdf (see attached gif file).

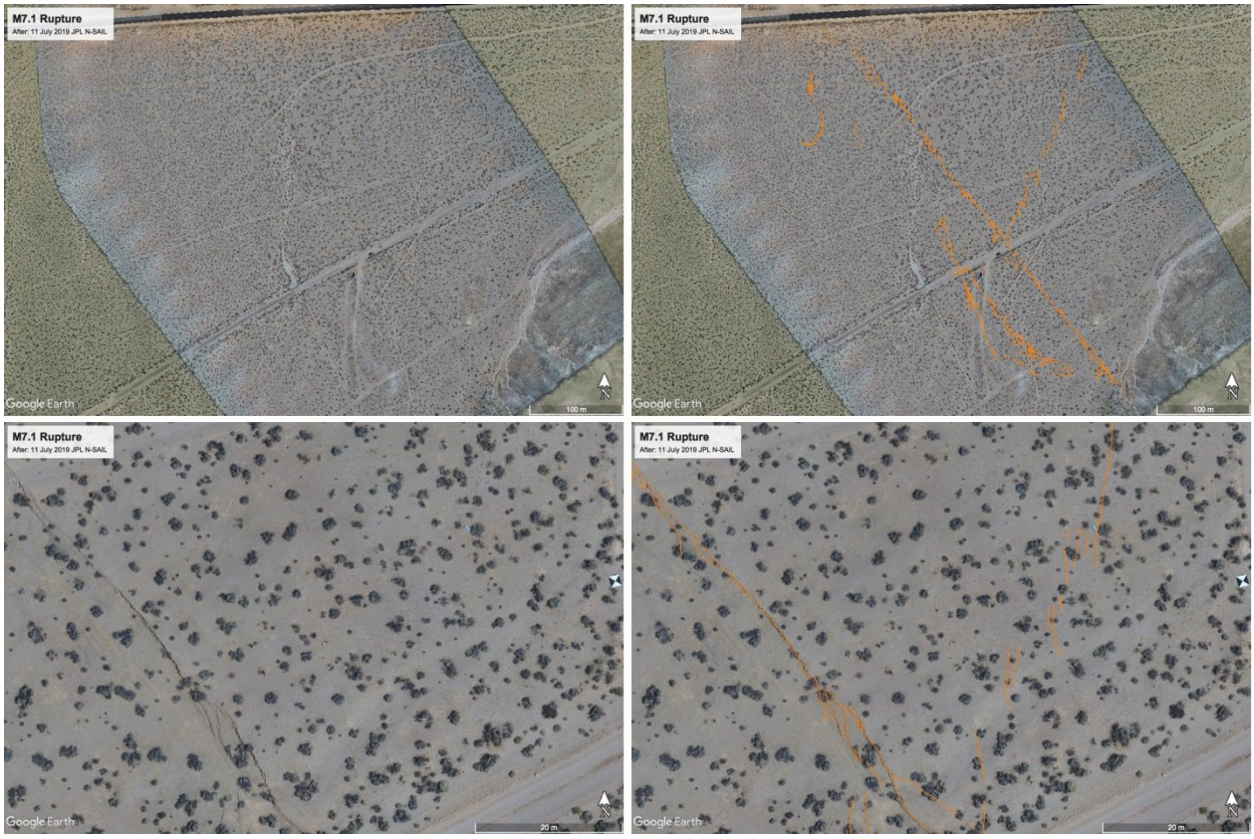

Figure 55. Images showing a portion of the detailed mapping area of the **M**7.1 rupture near line B5 as shown on Figure 21. Top row shows images at width of 100 m, bottom row shows zoomed portion of image at width of 20 m. Right side is image with locations of ruptures highlighted. JPL SfM initial image created on July 11 following their UAV flight showing the main fault strands as well as the distributed cracks in the rupture zone.

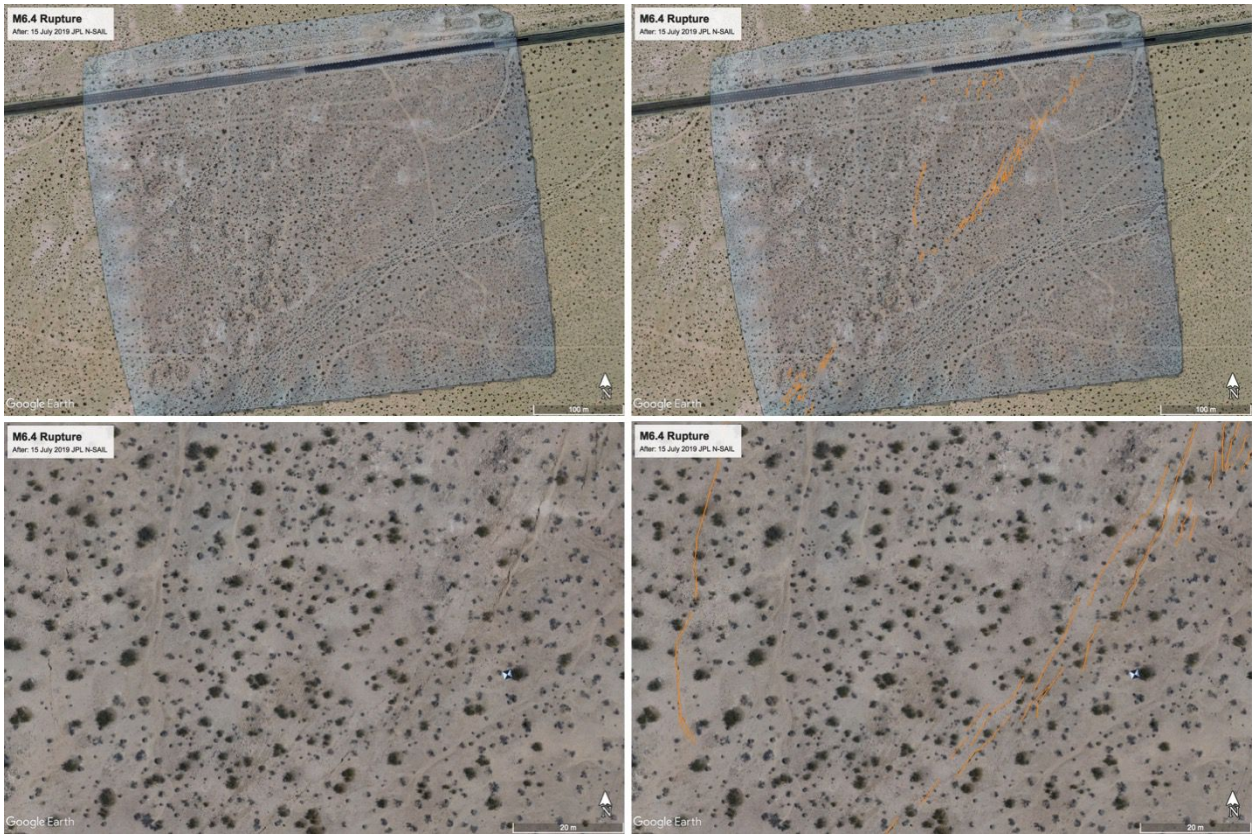

Figure 56. Similar to Figure 55, but for detailed mapping area of the **M**6.4 rupture immediately south of Highway 178 at location shown on Figure 25.

On July 10th, a group of UCLA researchers from Professor Timu Gallien's research group, and Scott Brandenberg, collected UAV images of the **M**7.1 surface rupture. Their survey started at the south-eastern limit of the JPL survey, and proceeded toward the southeast. Ground control points were surveyed and included in the images for the purpose of geo-referencing. The group imaged approximately 2km of the fault rupture. On July 11th, the same group of researchers collected UAV images in Trona and Argus, where liquefaction-induced lateral spreading occurred. The GEER team previously mapped these liquefaction features in Trona and Argus. Processing of the collected images is ongoing. Beginning July 16th, the NHERI Rapid facility centered at the University of Washington deployed to gather ground-controlled UAV images for the portion of the **M**6.4 surface rupture starting at the south-western limit of the JPL survey, and proceeding toward the southwest. This team was assisted by students from UCLA. The Trona Pinnacles site was also imaged.

The ground cracks formed by the surface rupture were observed to degrade during the two weeks following the earthquakes. For example, the UCLA team observed that vertical offsets in the fault rupture had collapsed into sloping features at many points along the surface rupture trace. Degradation was likely caused by a number of factors, including disturbance by people

due to foot and vehicular traffic, continued shaking from aftershocks, and wind-blow sands filling ground cracks. These observations underscore the importance of mobilizing quickly after an earthquake to gather perishable data.

3.2 Lidar

Ground-based lidar has been performed within the base along the fault, across a several kilometer long section where the fault crosses the China Lake playa surface. The USGS truck-mounted mobile lidar system (MLS) (Figure 56) was employed to generate DEM's of the offset lakebed surface that are nominally allowing creation of better than 3-5cm DEM's during initial processing (Figure 57). Higher resolution will be possible, given the point density of thousands of points per square meter along the rupture. Navy review of imagery-derived products is pending at this time.

Figure 56. USGS mobile lidar system truck in operation on the east side of the principal fault rupture in China Lake (dry). Photo credit: Ben Brooks, USGS.

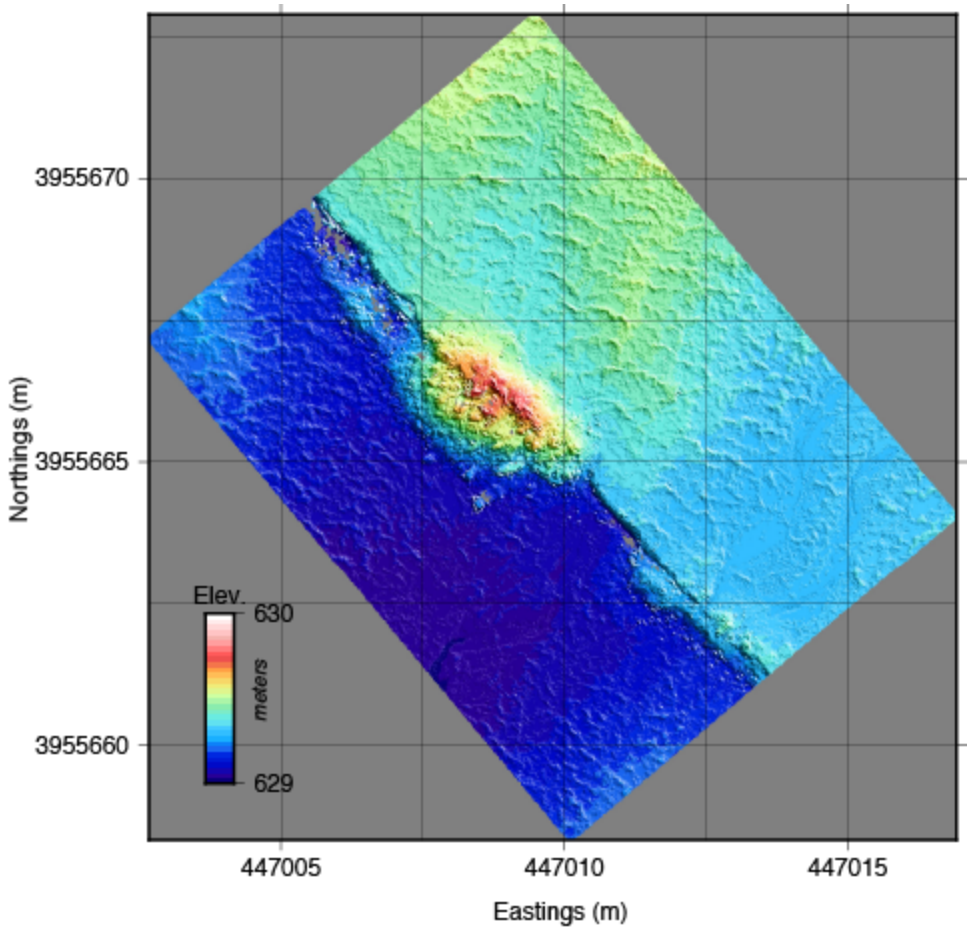

Figure 57. Example of USGS mobile lidar digital elevation model (DEM). DEM grid size is 2.5cm. The example shows the principal rupture on China Lake offsetting right-laterally, by approx. 1 m, a preexisting sand dune. Additionally the DEM shows vertical relief on the fault scarp on the order of ~25 cm. Grid graticules are 2.5 meters.

Airborne lidar is being proposed and planned for the entire rupture. A SCEC-led team that includes UC Davis, ASU, USGS and CGS has written an NSF Rapid proposal. The National Center for Airborne Laser Mapping (NCALM) will mobilize as early as July 26, 2019 to begin performing the scans if funding is approved.

4.0 DesignSafe Integration

The GEER team have utilized the DesignSafe cyberinfrastructure (Rathje et al. 2017) to store their photos and GPS track logs, and the HazMapper app to visualize the reconnaissance outcomes. Various GeoJSONfiles were created using the HazMapper app and saved in the following publicly accessible directory: Community Data / Recon Portal / 2019 Ridgecrest, CA Earthquake. Anyone with a DesignSafe account can launch HazMapper from the workspace,

and load the GeoJSONfiles stored in the community data folder. We envision that these resources will be useful for ongoing and future reconnaissance efforts.

References

Abrahamson, NA, Silva, WJ, and Kamai, R, 2014. Summary of the ASK14 fround motion relation for active crustal regions. *Earthquake Spectra,* 30, 1025-1055.

Ahdi, SK, Stewart, JP, Ancheta, TD, Kwak, DY, Mitra, D, 2017. Development of VS profile database and proxy-based models for VS30 prediction in the Pacific Northwest region of North America. *Bull. Seismol. Soc. Am.*, 107, 1781–1801.

Ancheta, TD, Darragh, RB, Stewart, JP, Seyhan, E, Silva, WJ, Chiou, BS-J , Wooddell, KE, Graves, RW, Kottke, AR, Boore, DM, Kishida, T, and Donahue, JL, 2014. NGA-West2 database. *Earthquake Spectra*, 30, 989-1005.

ASCE, 2010. *Minimum Design Loads for Buildings and Other Structures*. ASCE/SEI Standard 7-10.

Boore, DM, 2010. Orientation-Independent, nongeometric-mean measures of seismic intensity from two horizontal components of motion. *Bull. Seismol. Soc. Am.*, 100, 1830–1835.

Boore, DM, Stewart, JP, Seyhan, E, and Atkinson, GM, 2014. NGA-West2 equations for predicting PGA, PGV, and 5% damped PSA for shallow crustal earthquakes. *Earthquake Spectra*, 30, 1057-1085.

Brune, JN, 1996. Precariously balanced rocks and ground-motion maps for Southern California. B*ulletin of the Seismological Society of America*, 86 (1A): 43–54.

Bryant, WA, compiler, 2017. Fault number 72, Little Lake fault zone, in Quaternary fault and fold database of the United States: U.S. Geological Survey website, https://earthquakes.usgs.gov/hazards/qfaults, accessed 07/15/2019 04:04 PM.

Campbell, KW, and Bozorgnia, Y, 2014. NGA-West2 ground motion model for the average horizontal components of PGA, PGV, and 5% damped linear acceleration response spectra. *Earthquake Spectra*, 30, 1087-1115.

Chiou, BS-J and Youngs, RR, 2014. Update of the Chiou and Youngs NGA model for the average horizontal component of peak ground motion and response spectra. *Earthquake Spectra*, 30, 1117-1153.

Hanks, TC and Allen, CR 1989. The Elmore Ranch and Superstition Hills earthquakes of 24 November 1987: Introduction to the Special Issue, *Bull. Seis. Soc. Amer.*, 79, 231-238.

Hudnut, KW, Seeber, L, and Pacheco, J, 1989. Cross-fault triggering in the November 1987 Superstition Hills earthquake sequence, southern California, *Geophys. Res. Lett.*, v. 16 #2, p. 199-202.

IRIS, 2019a. Mw 6.4 CENTRAL CALIFORNIA Event Page, *Incorporated Research Institutions for Seismology (IRIS) Searchable Product Depository (SPUD)*; http://ds.iris.edu/spud/event/11056847, last accessed 2019-07-16.

IRIS, 2019b. Mw 7.1 CENTRAL CALIFORNIA Event Page, *Incorporated Research Institutions for Seismology (IRIS) Searchable Product Depository (SPUD)*; https://ds.iris.edu/spud/event/11058875, last accessed 2019-07-16.

Iwahashi, J and Pike, RJ, 2007. Automated classifications of topography from DEMs by an unsupervised nested-means algorithm and a three-part geometric signature, *Geomorphology*, 86, 3–4, pp. 409-440.

Mosalam, K, Lead Author, 2019. M 6.4 and M 7.1 Ridgecrest, CA Earthquakes Preliminary Virtual Reconnaissance Report, Structural Extreme Event Reconnaissance, NHERI DesignSafe Project ID: PRJ-2444.

Rathje, EM, Dawson, C, Padgett, JE, Pinelli, J-P, Stanzione, D, Adair, A, Arduino, P, Brandenberg, SJ, Cockeril, T, Esteva, M, Haan, FL Jr., Hanlon, M, Kareem, A, Lowes, L, Mock, S, and Mosqueda, G, 2017. DesignSafe: A new cyberinfrastructure for natural hazards engineering. *Natural Hazards Review*. 18(3).

Seyhan, E, Stewart, JP, Ancheta, TD, Darragh, RB, and Graves, RW, 2014. NGA-West2 site database. *Earthquake Spectra*, 30, 1007-1024.

Smith, GI, 2009. Late Cenozoic geology and lacustrine history of Searles Valley, Inyo and San Bernardino Counties, California: U.S. Geological Survey Professional Paper 1727, 115 p., 4 plates.

Thompson, EM, 2018. An Updated Vs30 Map for California with geologic and topographic constraints: U.S. Geological Survey data release, https://doi.org/10.5066/F7JQ108S.

Wills, CJ, 1988. Little Lake and Airport Lake fault zones, Inyo and Kern counties, California, California Division of Mines and Geology Fault Evaluation Report 199, 10 p., 7 maps, scale 1:24,000.

Wills, CJ, Gutierrez, CI, Perez, FG, and Branum, DM, 2015. A next generation VS30 map for California based on geology and topography. *Bull. Seismol. Soc. Am.*, 105, 3083–3091.

USGS and CGS, 2019. Quaternary fault and fold database for the United States, accessed 7/13/2019, from USGS web site: https://earthquake.usgs.gov/hazards/qfaults/.

Yong, A, 2016. Comparison of measured and proxy-based VS30 values in California. *Earthquake Spectra,* 32, 171-192.

Recommended Citation:

Stewart, J.P. (ed.), Brandenberg, S.J., Wang, Pengfei, Nweke, C.C., Hudson, K., Mazzoni, S., Bozorgnia, Y., Hudnut, K.W., Davis, C.A., Ahdi, S.K., Zareian, F., Fayaz, J., Koehler, R.D., Chupik, C., Pierce, I., Williams, A., Akciz, S., Hudson, M.B., Kishida, T., Brooks, B.A., Gold, R.D., Ponti, D.J., Scharer, K.M., McPhillips, D.F., Ericksen, T.., Hernandez, J., Patton, J., Olson, B., Dawson, T., Treiman, J., Duross, C.B., Blake, K., Buchhuber, J., Madugo, C., Sun, J., Donnellan, A., Lyzenga, G., and Conway, E., 2019, Preliminary report on engineering and geological effects of the July 2019 Ridgecrest Earthquake sequence: Geotechnical Extreme Events Reconnaissance Association Report GEER-064, https://doi.org/10.18118/G6H66K.